

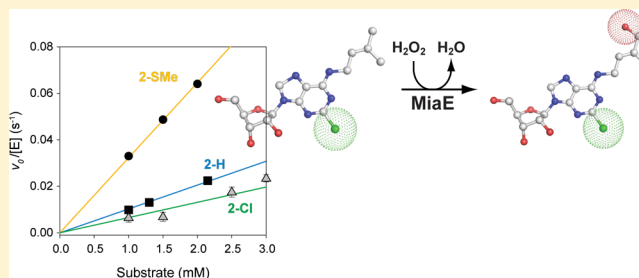
Peroxide-Shunt Substrate-Specificity for the *Salmonella typhimurium* O₂-Dependent tRNA Modifying Monooxygenase (MiaE)

Andra L. Corder,^{†,‡} Bishnu P. Subedi,[†] Siai Zhang,[†] Amanda M. Dark,[‡] Frank W. Foss, Jr.,^{*,‡} and Brad S. Pierce^{*,†}

[†]Biophysical/Bioinorganic Group and [‡]Synthetic Organic Group, Department of Chemistry and Biochemistry, College of Science, The University of Texas at Arlington, Arlington, Texas 76019, United States

Supporting Information

ABSTRACT: Post-transcriptional modifications of tRNA are made to structurally diversify tRNA. These modifications alter noncovalent interactions within the ribosomal machinery, resulting in phenotypic changes related to cell metabolism, growth, and virulence. MiaE is a carboxylate bridged, nonheme diiron monooxygenase, which catalyzes the O₂-dependent hydroxylation of a hypermodified-tRNA nucleoside at position 37 (2-methylthio-N⁶-isopentenyl-adenosine(37)-tRNA) [designated ms²i⁶A₃₇]. In this work, recombinant MiaE was cloned from *Salmonella typhimurium*, purified to homogeneity, and characterized by UV-visible and dual-mode X-band EPR spectroscopy for comparison to other nonheme diiron enzymes. Additionally, three nucleoside substrate-surrogates (i⁶A, Cl²i⁶A, and ms²i⁶A) and their corresponding hydroxylated products (io⁶A, Cl²io⁶A, and ms²io⁶A) were synthesized to investigate the chemo- and stereospecificity of this enzyme. In the absence of the native electron transport chain, the peroxide-shunt was utilized to monitor the rate of substrate hydroxylation. Remarkably, regardless of the substrate (i⁶A, Cl²i⁶A, and ms²i⁶A) used in peroxide-shunt assays, hydroxylation of the terminal isopentenyl-C4-position was observed with >97% *E*-stereoselectivity. No other nonspecific hydroxylation products were observed in enzymatic assays. Steady-state kinetic experiments also demonstrate that the initial rate of MiaE hydroxylation is highly influenced by the substituent at the C2-position of the nucleoside base ($v_0/[E]$ for ms²i⁶A > i⁶A > Cl²i⁶A). Indeed, the >3-fold rate enhancement exhibited by MiaE for the hydroxylation of the free ms²i⁶A nucleoside relative to i⁶A is consistent with previous whole cell assays reporting the ms²io⁶A and io⁶A product distribution within native tRNA-substrates. This observation suggests that the nucleoside C2-substituent is a key point of interaction regulating MiaE substrate specificity.



Post-transcriptional modifications of transfer-RNA (tRNA) have been identified across all phylogenetic domains of life (Archaea, Bacteria, and Eucarya).¹ Ironically, more genes are devoted to enzymes involved in the modification of tRNA nucleosides than to the various tRNA genes themselves.^{1,2} These modifications are made to structurally diversify tRNA from the four canonical nucleoside building blocks [adenosine, (A); guanosine, (G); uridine, (U); and cytosine, (C)].³ At present, nearly 90 structurally unique nucleoside modifications have been identified in tRNA.¹ In many instances, the physiologic role of such modifications is unclear; however, several examples have been identified to suggest that the presence of modified nucleosides in tRNA can impact central metabolism (*citric acid cycle*), thiamine biosynthesis, and bacterial virulence.⁴ Of these modifications, perhaps the best understood are those localized within the anticodon stem loop (ASL).⁵ Specific modifications within the ASL region of tRNA have been shown to improve aminoacyl-tRNA selection, regulate gene expression, and decrease translational frame-shifting.¹

Within the ASL, the majority of nucleoside modifications occur at either position 34 (the wobble position) or position 37

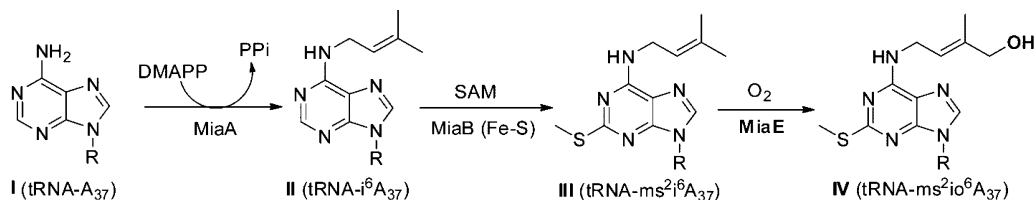
(3' adjacent to anticodon).⁴ In many instances, modification of the nucleoside involves a single chemical step such as the addition of a methyl or methylthiol group to the base. Alternatively, some modifications employ multiple enzymes within a complex biochemical pathway to produce a hypermodified nucleoside. Scheme 1 illustrates a particularly interesting hypermodification pathway which occurs at adenine-37 (A₃₇) within the ASL. In facultative anaerobes such as *S. typhimurium*, the extent of A₃₇-modification is believed to regulate aromatic amino acid uptake, enterochelin synthesis, iron transport, and aerobiosis.^{3,4,6}

In the first reaction shown in Scheme 1, dimethylallyl (Δ²-isopentyl) diphosphate-tRNA transferase [E.C. 2.5.1.8] (designated MiaA) catalyzes the nucleophilic substitution of the dimethylallyl group from dimethylallyl pyrophosphate (DMAPP) to the exocyclic 6-amino nitrogen of A₃₇ (N⁶) to yield N⁶-isopentenyl-adenosine (i⁶A₃₇) with release of inorganic pyrophosphate.⁸ The second enzymatic transformation involves

Received: January 22, 2013

Revised: July 31, 2013

Published: August 1, 2013

Scheme 1. Hypermodification Pathway for $ms^2io^6A_{37}$ 

the formal methylthiolation of i^6A_{37} at the C2-position to produce 2-methylthio- N^6 -isopentenyl-adenosine ($ms^2i^6A_{37}$). The enzyme that catalyzes this remarkable transformation (2-methylthio- N^6 -isopentenyl-adenosine synthase, designated MiaB) requires S-adenosylmethionine⁹ as a co-substrate and is a member of the “radical-SAM” iron–sulfur super family of enzymes.^{9,10} With the notable exception of tRNA_{I,V}^{Ser(GGA)}, nearly all eukaryotic and bacterial tRNAs that read codons starting with U contain the ms^2i^6A -modification.^{1,3} The final enzyme in this pathway (MiaE, 2-methylthio- N^6 -isopentenyl-adenosine(37)-tRNA monooxygenase) catalyzes the O_2 -dependent hydroxylation of $ms^2i^6A_{37}$ to produce 2-methylthio- N^6 -(4-hydroxyisopentenyl)-adenosine ($ms^2io^6A_{37}$).¹¹ While MiaE can utilize i^6A_{37} as a substrate, whole cell assays suggest a preference for $ms^2i^6A_{37}$.^{12–14} MiaA and MiaB are common in both eukaryotes and prokaryotes; however, MiaE is found only within a small subset of facultative anaerobic bacteria such as *Salmonella typhimurium*, *Rhizobium leguminosarum*, *Corynebacterium fascians*, and *Agrobacterium tumefaciens*.^{15,16} Interestingly, *Salmonella typhimurium* mutants lacking MiaE are unable to grow on citric acid cycle intermediates succinate, fumarate, or malate.¹⁷ These *miaE*[−] mutants do not exhibit decreased catalytic activity or expression of citric acid cycle enzymes. Furthermore, their uptake of dicarboxylic acids is also unaffected.¹⁷ Based on these observations, it has been suggested that *Salmonella typhimurium* utilizes the hypermodified $ms^2io^6A_{37}$ as a signal for the availability of molecular oxygen. Thus, $ms^2io^6A_{37}$ may serve as a means to help regulate aerobiosis.^{1,7,13}

Sequence alignment and spectroscopic characterization (EPR/Mössbauer) of MiaE indicate that it is a member of the nonheme diiron family of enzymes.^{11,16} Other members of this family include the hydroxylase components of the bacterial multicomponent monooxygenases [methane monooxygenase (MMOH), toluene-monooxygenases (ToMOH)], the small subunit of ribonucleotide reductase (R2), and stearyl-acyl carrier protein Δ^9 -desaturase ($\Delta 9D$).^{18–20} The study of nonheme enzymes and model complexes has historically attracted considerable interest in the realm of bioinorganic chemistry. This intense focus of research efforts can largely be explained by the vast number of functionally (and structurally) diverse nonheme diiron enzymes identified throughout the biological kingdom and the incredible versatility exhibited in chemical oxidations (mono- and dioxygenations, aliphatic desaturation) they initiate. Remarkably, all of these divergent oxidations are facilitated by minor perturbations to what is essentially a conserved first-coordination sphere to the diiron cluster. The mechanistic paradigm for this class of enzymes starts with the 2 electron reduction of the resting diferric center to produce a diferrous cluster. The diferrous center can then react with molecular oxygen to produce a high-valent oxidizing species capable of substrate oxidation.^{11,21–23} For example, the hydroxylase component of methane monooxygenase (MMOH)

from *Methylococcus capsulatus* (Bath) is one of the most extensively characterized nonheme diiron enzymes.^{24–26} In this enzyme, a high-valent diferryl iron species, termed compound Q, has been identified as the oxidizing intermediate responsible for substrate oxidation.^{27,28} Alternatively, a diferric peroxo species has been proposed to be the catalytically competent intermediate in the ToMOH-catalyzed oxidation of aromatic hydrocarbons.²⁹ As with heme oxidase enzymes, many nonheme diiron enzymes exhibit a ‘peroxide-shunt’ pathway in which the high-valent substrate-oxidizing intermediate can be produced by addition of hydrogen peroxide to the resting diferric enzyme. This pathway removes the need for an external electron source, but frequently at the cost of product yield and specificity.^{18,19,21}

In this work, three nucleoside substrate surrogates [N^6 -isopentenyl-adenosine (i^6A); 2-methylthiol- N^6 -isopentenyl-adenosine, (ms^2i^6A); and 2-chloro- N^6 -isopentenyl-adenosine, (Cl^2i^6A)] were synthesized such that the chemo- and stereospecificity of recombinant MiaE cloned from *Salmonella typhimurium* could be examined. In these assays, the nonheme diiron peroxide-shunt was used in lieu of the native electron-transport chain to perform steady-state kinetic assays.³⁰ Both the (Z)- and (E)-isomers of the hydroxylated products [N^6 -(4-hydroxyisopentenyl)-adenoside (io^6A); 2-methylthiol- N^6 -(4-hydroxyisopentenyl)-adenoside (ms^2io^6A); 2-chloro- N^6 -(4-hydroxyisopentenyl)-adenoside (Cl^2io^6A)] were synthesized for standards in HPLC enzymatic assays and confirmation of MiaE product stereochemistry. Remarkably, for all synthetic nucleosides, MiaE was capable of chemo- and stereoselective *E*-hydroxylation at the terminal C4-position of the isopentenyl-amine-group. Moreover, the results obtained from kinetic experiments suggest that, even in the absence of macromolecular tRNA:MiaE interactions, the C2-position greatly effects the second order reaction rate. Perhaps coincidentally, the observed initial rate is proportional to positive substituent effects at the C2-position ($-SMe > -H > -Cl$). This observation is consistent with the observation that MiaE preferential hydroxylates ms^2i^6A - over i^6A -tRNA *in vivo*.¹³

■ MATERIALS AND METHODS

Cloning. The *miaE* gene was isolated from *Salmonella enterica* strain LT2 genomic DNA [ATCC 700720] using primers purchased from Integrated DNA Technologies (<https://www.idtdna.com>). A two-step PCR amplification was used to isolate the ORF from genomic DNA and incorporate restriction sites (Sgf I/Pme I) for Flexi-vector cloning (Promega, Madison, WI), followed by insertion of a recognition site for tobacco etch virus protease (TEV). First, (*miaE* specific) PCR reaction primers: forward 5'-(AAC CTG TAC TTC CAG TCC AAT TAC CCG CAA ATA CTC TCT CCG G)-3'; reverse 5'-(GCT CGA ATT CGT TTA AAC TAT CCG GCG GCT GGC ACG CCG CTA TG)-3'. Second (TEV site insertion) primers: forward: 5'-(GGT TGC GAT

CGC CGA AAA CCT GTA CTT CCA GTC C)-3'; reverse: 5'-(GTG TGA GCT CGA ATT CGT TTA AAC)-3'. The DNA produced by this two-step PCR amplification was cloned into an isopropyl β -D-1-thiogalactopyranoside (IPTG) inducible T7 vector (designated pVP80K) obtained from the University of Wisconsin, Center for Eukaryotic Structural Genomics (UW CESG). Sequence verification of *miaE* was performed in the life sciences department at UTA by the Genomics Core Facility (http://gcf.uta.edu/Core_Facility/Core_Facility.html). The resulting plasmid (pMIAE80K) expresses an N-terminal fusion of maltose binding protein (MBP) and MiaE. The two proteins are separated by a recognition sequence for tobacco etch virus (TEV) protease such that cleavage of the two proteins can be performed following purification. (NOTE: Within the ORF for the *miaE* gene, two possible start codons are present.¹¹ However, only constructs generated from the second start codon resulted in a soluble (29 kDa) protein product.)

For *in vivo* MiaE activity assays, a second 'untagged' MiaE construct (pMIAEK) was cloned into the commercially available pF1K flexi-vector (Promega). PCR primers: *Sfg I*-forward; 5'-(TTT AAC AGC GAT CGC ATG AAT TAC CCG CAA ATA)-3'; *Pme I*-reverse; 5'-(GTG GTG TTT AAA CTT ATC CGG CGG CTG GCA CGC CGC)-3'. Forward and reverse restriction sites are underlined for clarity. Sequence verification was performed as described above. Expression of soluble protein (29 kDa) was confirmed by SDS PAGE. (NOTE: BL21(DE3) *E. coli* cells transformed with the 'untagged' MiaE vector (pMIAEK) have a significantly lower growth rate (~2-fold) in LB-media as compared to cells transformed with the MBP-tagged vector (pMIAE80K). Moreover, cells transformed with pMIAEK showed a significant decrease in cell growth upon induction. This was partly remedied by decreasing the induction temperature from 25 to 17 °C and increasing the time before harvesting cells. We speculate that the N-terminal MBP-tag attenuates promiscuous activity of MiaE within *E. coli* during basal expression. For this reason, the pMIAEK vector was used only for *in vivo* activity confirmation where as the pMIAE80K vector was used for overexpression, purification, and *in vitro* enzymatic assays.)

Media and Growth Conditions. The pMIAE80K vector was transformed into chemically competent BL21(DE3) *E. coli* (Novagen) by heat-shock and grown overnight at 37 °C on a lysogeny broth (LB)³¹ agar plate in the presence of 25 μ g/mL Kanamycin (Kan). The following day, a single colony was selected for growth in liquid LB (Kan) media for training on antibiotic prior to inoculation of 10-L BF-110 fermentor (New Brunswick Scientific) at 37 °C. Cell growth was followed by optical density at 600 nm (OD₆₀₀). Induction was initiated by addition of 0.5 mM IPTG, 1 mM ferrous ammonium sulfate, and 20 g casamino acids at an OD₆₀₀ ~4. Additionally, upon induction the temperature of the bioreactor was decreased from 37 to 25 °C and agitation was set to maintain an O₂ concentration of 20% relative to air-saturated media. After 4 h of induction, the cells were pelleted by centrifugation (Beckman-Coulter Avanti J-E, JA 10.5 rotor) at 18 600 \times g for 15 min, and the paste was stored at -80 °C. Confirmation of MiaE expression was performed by SDS-PAGE of lysed cells before and after IPTG induction.

Protein Purification. Approximately 25 g of cell paste was suspended in 50 mL of lysis buffer (20 mM HEPES, 40 mM NaCl, pH 8.0), and thawed in an ice bath with 10 μ g/mL each of lysozyme, deoxyribonuclease I, and ribonuclease with gentle

stirring for 30 min. The cell suspension was sonicated in a 30 s on/off pulse cycle for a total of 10 min. The resulting cell free extract was centrifuged (JA 20 rotor) at 48 000 \times g for 60 min at 4 °C. The supernatant was loaded onto a fast flow DEAE column pre-equilibrated in lysis buffer, and the protein was eluted on a linear NaCl gradient (40 mM to 350 mM NaCl in 20 mM HEPES, 0.3 mM Tris[2-carboxyethyl] phosphine (TCEP), pH 8.0). The fractions containing the MBP-MiaE protein, determined by SDS-PAGE, were concentrated via Amicon N₂ stir cell equipped with an YM 30 ultrafiltration membrane. TEV protease was used to cleave the fusion protein by overnight storage at 4 °C. The cleaved fusion protein was desalted by dialysis (Spectra/por, Spectrum Laboratories Inc.) in lysis buffer. To separate MBP from MiaE enzyme, the desalted protein was reloaded through the DEAE Sepharose column equilibrated in lysis buffer. The protein was eluted on a linear NaCl gradient (0 mM to 350 mM NaCl in 20 mM HEPES, pH 8.0) and fractions containing only MiaE were identified by SDS PAGE and UV-visible spectroscopy. Stoichiometric iron incorporation in purified MiaE was verified by UV-visible spectroscopy on the basis of the Fe-associated bands typically observed between 320 and 380 nm. Only fractions with $A_{280}/A_{370} \sim 7.8 \pm 0.3$ were pooled and concentrated (YM 10 ultra membrane) for use in experiments. For the purified MiaE enzyme, the published extinction coefficient at 280 nm (60 000 M⁻¹ cm⁻¹) was used to quantify protein samples.¹¹ Within experimental error (5–10%), determination of protein concentration by UV-visible spectroscopy and standard Bio-Rad protein assay (Bio-Rad Laboratories Inc.) were equivalent.

TEV Purification and Cleavage Conditions. The TEV expression vector (pMHT Δ 238) was a generous gift from Dr. Russell Wrobel and Professor Brian G. Fox (UW CESG). Expression and cell growth were performed as described for pMIAE80K. Approximately 10 g of TEV cell paste was thawed in 20 mL of IMAC buffer A (20 mM NaH₂PO₄, 500 mM NaCl, 1 mM β -mercaptoethanol, pH 7.5) in an ice bath for 30 min. The suspension containing 10 μ g/mL each of lysozyme, deoxyribonuclease I, and ribonuclease was pulse sonicated for 10 min, and centrifuged in a 48 000 \times g (JA 20 rotor) for 60 min. The supernatant was collected and loaded onto a 5-mL Hi-Trap immobilized metal affinity chromatography (IMAC) column (GE Healthcare) pre-equilibrated in IMAC buffer A. The column was washed with 5 column volumes (25 mL) of IMAC buffer A prior to elution of TEV enzyme with 2 column volumes of IMAC buffer B (350 mM imidazole in IMAC A, pH 7.5). Excess imidazole was removed by dialysis (Spectra/por, Spectrum Laboratories Inc.) in IMAC buffer A. An Amicon N₂ stir cell equipped with YM-10 ultrafiltration membrane was used to concentrate the TEV protease. Aliquots (1 mL) of TEV were stored at 1 mg/mL in 50% glycerol at -20 °C. For a typical cleavage reaction, eq 1 OD₂₈₀ of TEV protease was used per 5 OD₂₈₀ of MBP-MiaE fusion protein.

Iron Quantitation. The total iron present in the protein sample was quantitated by using UV-visible spectrophotometer according to published method.³² Typically, a 500 μ L protein sample was denatured with 250 μ L each of hydrochloric acid (2N) and trichloroacetic acid (20%). All iron released from the denatured protein was reduced to ferrous iron by addition of 100 μ L hydroxylamine hydrochloride (10% w/v). 200 μ L of 2,4,6-tripyridyl-S-triazine (TPTZ) (4 mM) was added as a chromophore along with 100 μ L of ammonium acetate solution (50% w/v). A UV-visible spectrophotometer was used to

measure the intense color produced by coordination of ferrous iron by TPTZ ($\epsilon_{596} = 22\,600\text{ M}^{-1}\text{ cm}^{-1}$). The concentration of adventitious ferric iron ($S = S/2$) was determined by X-band (9 GHz) Bruker EPR spectrometer³³ by double integration of the observed signal at $g = 4.3$ ($B_{\perp} \perp B$) and comparison to a known Cu^{II} -standard.

Analytical Ultracentrifugation. The native molecular weight, oligomeric state, and sedimentation coefficient of purified MiaE was determined by Virgil Schirf (schirfv@biochem.uthscsa.edu) and Borries Demeler (demeler@biochem.uthscsa.edu) at the UT Health Science Center (San Antonio, TX), Center for Analytical Ultracentrifugation of Macromolecular Assemblies (CAUMA, <http://www.cauma.uthscsa.edu/>). Three samples (500 μL) of purified MiaE were prepared at 4.7, 9.3, and 15.5 μM within 20 mM HEPES, 100 mM NaCl, pH 8.0 for sedimentation analysis. The monomeric state of MiaE was confirmed by both genetic algorithm and Monte Carlo analysis.^{34,35}

Calibration of Sodium Dithionite Solutions. All anaerobic samples were prepared in a glovebox (Coy Laboratory Products Inc., Grass City, MI) with the O_2 concentration maintained below 1 ppm. Solutions utilized for reductive titration were prepared in the standard MiaE buffer (20 mM HEPES, 40 mM NaCl, pH 8.0) degassed on a Schlenk line prior to transferring into the anaerobic chamber. Analytical grade argon was passed through a copper catalyst (Kontes, Vineland, NJ) to remove trace O_2 impurities and then sparged through distilled water to hydrate the gas. Sodium dithionite is highly sensitive to degradation due to atmospheric moisture and oxygen. Therefore, the amount of 'reducing equivalents' within each stock solution must be analytically determined by titration with potassium ferricyanide prior to use. The 1-electron reduction of the ferricyanide anion can be followed spectrophotometrically at 420 nm [$\epsilon_{(420)} = 1050\text{ M}^{-1}\text{ cm}^{-1}$] as described in Supporting Information. Therefore, in reductive titrations the value of 'reducing equivalents' is reported as opposed to the concentration of sodium dithionite.

Catalase Activity. An oxygen electrode was used to measure the rate of oxygen produced upon H_2O_2 addition to enzyme solutions to measure the low-level catalase activity of MiaE.^{11,36} Dioxygen concentration was determined polarographically using a standard Clark electrode (Hansatech Instruments, Norfolk, England) within a jacketed 2.5-mL cell at $25 \pm 2\text{ }^\circ\text{C}$. The electrode was bathed in a saturated solution of KCl and separated from the buffer using a gas-permeable membrane. The electrode was calibrated by measuring the deflection in the voltage upon adding ~ 500 units of catalase (Sigma-Aldrich, St. Louis) to a buffer with a known concentration of H_2O_2 [$\epsilon_{(250)} = 16.7\text{ M}^{-1}\text{ cm}^{-1}$]. Confirmation of initial hydrogen peroxide concentration in buffered solutions was performed using the amplex red hydrogen peroxide/peroxidase kit for spectrophotometric determination ($\lambda = 560\text{ nm}$) of H_2O_2 (Invitrogen, cat. no. A22188). Once the reaction reached completion, the amplitude for the change in voltage was used to determine a response factor for the electrode. The reaction was initiated by injection of MiaE resulting in final enzyme concentration of 5 μM .

Spectroscopy. All UV-visible measurements were performed on an Agilent 8453 photo diode array spectrometer (Santa Clara, CA). Sample temperature was held constant by a 13 L circulating water bath and a thermostatable cell holder (89054A) with magnetic stirrer. All measurements were made in ES Quartz cuvettes (NSG Precision Cells, Farmingdale, NY).

X-band (9 GHz) EPR spectra were recorded on a Bruker (Billerica, MA) EMX Plus spectrometer equipped with a bimodal resonator (Bruker model 4116DM). Low-temperature measurements were made using an Oxford ESR900 cryostat and an Oxford ITC 503 temperature controller. A modulation frequency of 100 kHz was used for all EPR spectra. All experimental data used for spin-quantitation were collected under nonsaturating conditions.

For simulations of the reduced diiron cluster, it was assumed that the exchange coupling constant (J) is comparable in energy to (or larger) than the zero-field splitting (D) of the diferrous cluster. Under this constraint, the $S = 4$ Hamiltonian takes the form illustrated in eq 1.

$$\hat{H} = D \left(\hat{S}_Z^2 - \frac{S(S+1)}{3} \right) + E(\hat{S}_X^2 + \hat{S}_Y^2) + \beta \mathbf{B} \cdot \mathbf{g} \cdot \mathbf{S} \quad (1)$$

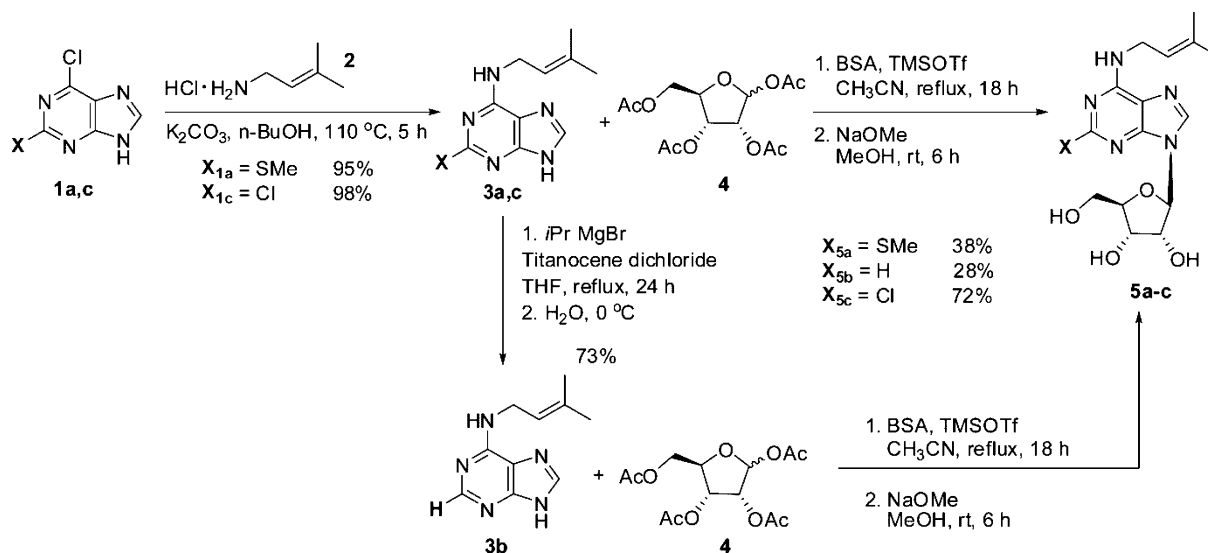
where D and E are the axial and rhombic zero-field splitting (zfs) parameters and \mathbf{g} is the g -tensor.³⁷ EPR spectra were simulated and quantified using Spin Count (v 3.1.2), written by Professor M. P. Hendrich at Carnegie Mellon University. The simulations were generated with consideration of all intensity factors, both theoretical and experimental, to allow for determination of species concentration. The only unknown factor relating the spin concentration to signal intensity was an instrumental factor that is specific to the microwave detection system. However, this was determined by the spin standard, $\text{Cu}(\text{EDTA})$, prepared from a copper atomic absorption standard solution purchased from Sigma-Aldrich.

Qualitative TLC Activity Assays. For initial substrate screening, TLC (thin layer chromatography) was utilized to analyze product formation. At selected time points, 10 μL of sample aliquots were removed, heat denatured, and cooled to $0\text{ }^\circ\text{C}$. The reaction mixture (1 μL) was spotted onto an EMD silica gel 60 F_{254} TLC plate (VWR) alongside 5.8 mM of the appropriate standard. After spotting the sample on the TLC plate, a heat-gun was used to completely dry the plate prior to elution. The TLC plate was eluted in 15% methanol in dichloromethane, dried with a heat gun, and stained in potassium permanganate for assay analysis.

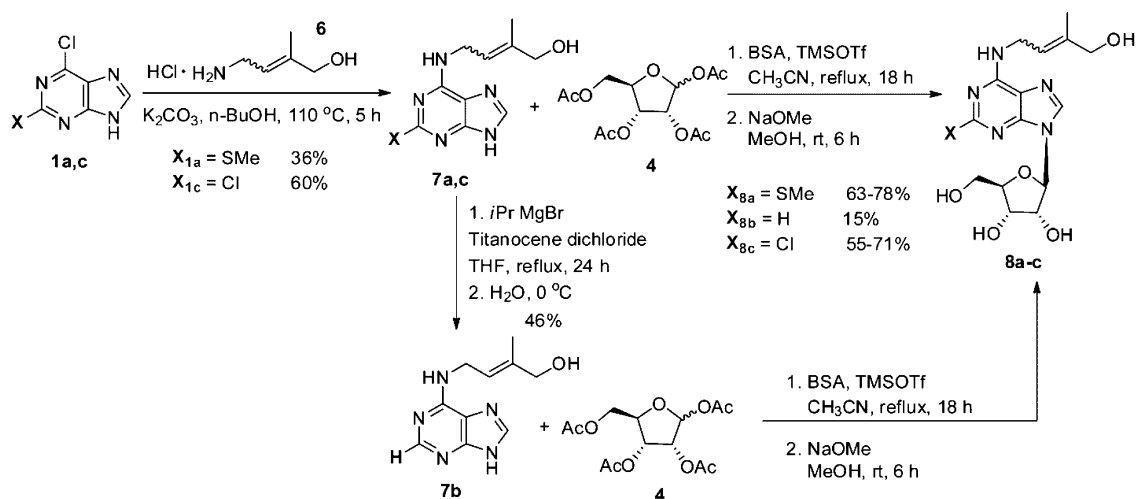
In Vivo Activity Assay. In a typical experiment, duplicate cultures (1 L each) of *E. coli* BL21(DE3) transformed with the untagged MiaE expression vector (pMIAEK) were grown in LB (25 $\mu\text{g}/\text{mL}$ kanamycin) at $37\text{ }^\circ\text{C}$ as described above. As a control, a separate culture of *E. coli* BL21(DE3) transformed with the TEV expression vector (pMHT Δ 238) was prepared for comparison. Upon reaching $\text{OD}_{600} \sim 0.8$, one culture was harvested and the cells collected by centrifugation; this 'preinduction' control sample was prepared for comparison cultures following IPTG-induction. The remaining two cultures transformed with pMIAEK and pMHT Δ 238 were induced by addition of 0.5 mM IPTG, 2 g/L casamino acids, $1\times$ Fe-solution (50 μM), and allowed to express for an additional 4 h at $25\text{ }^\circ\text{C}$ prior to harvesting by centrifugation.

Total RNA was recovered by phenol extraction and ethanol precipitation as described previously.^{11,38} Briefly, RNA was extracted from the cell free extract solution by addition of an equal volume of phenol:chloroform (5:1). Following vortex-mixing, the aqueous phase containing RNA was recovered. This process was repeated 3 times. The pooled aqueous extracts were then mixed with 2.5 volumes of ethanol and stored on ice to precipitate RNA. After 2 h on ice, the RNA pellet was recovered, dried, and reconstituted in autoclaved MQ H_2O .

Scheme 2. Synthetic Route of MiaE Analogs



Scheme 3. Synthetic Route of MiaE Modified Analogs

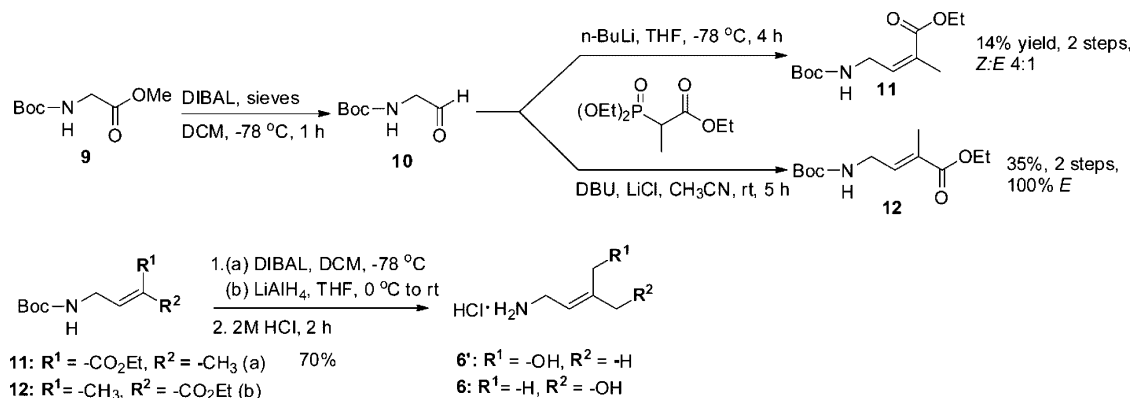


Since both ms^2i^6A and ms^2io^6A are relatively hydrophobic, $LiCl$ washes were not utilized to fractionate tRNA from rRNA.³⁹ From each culture (preinduced, IPTG induced MiaE, and IPTG induced TEV), samples of total RNA were hydrolyzed by nuclease P1 (Sigma Aldrich, Cat. No. N8630) and then dephosphorylated using bacterial alkaline phosphatase, (Invitrogen, Cat. No. 18011-015) according to published methods.^{11,40} The resulting samples were analyzed by reverse phase HPLC using the method developed by Gehrke et al.⁴⁰ HPLC instrumentation: Shimadzu quaternary pump LC (LC-20AD XR/LC 30AD) equipped with a diode array photodiode array detector (SPD-M20A); Column, Phenomenex, Gemini-NH $3\ \mu m$ C18 110 Å; $150\text{ cm} \times 4.6\text{ mm}$; Mobile phase, (A) 2.5% methanol in 0.01 M $NH_4H_2PO_4$; pH 5.1, (B) 20% methanol in 0.01 M $NH_4H_2PO_4$; pH 5.3, (C) 35% acetonitrile in 0.01 M $NH_4H_2PO_4$; pH 4.9; Injection volume, $50\ \mu L$; Flow rate, 1 mL/min ; Column temperature, $25\text{ }^\circ C$; UV-visible detection wavelength (254 nm).

In Vitro HPLC Activity Assays. Given the decreased number of nucleoside analytes present in peroxide-shunt enzymatic assays, the reverse-phase HPLC method and column was modified from that used in whole cell *in vivo* assays to

decrease the retention times.^{8,11,40} Therefore, attention was turned toward the use of a hydrophilic interaction liquid chromatography (HILIC) column (AZYP Frulic-N). It was found that with an isocratic elution of 98% acetonitrile and 2% aqueous buffer comprised of 2% triethylamine, 3% acetic acid at a rate of 2 mL/min , the HILIC column gave much shorter retention times, while maintaining baseline separation. Numerous samples were injected without any sign of column degradation or clogging. Substrate retention times ranged from 4 to 6 min, while product retention times ranged from 10 to 16 min. The reliability of the HILIC column was tested for *in vitro* assays, giving results within 5% of those obtained by C18 column. Therefore, this method provided equivalent resolution of peaks with a significantly shorter run time.

LC-MS/MS and Data Analysis. Verification of enzymatic product was performed by multiple reaction monitoring (MRM) using a triple quadrupole LC-MS/MS [Shimadzu Scientific Instruments, LCMS 8040].⁴¹ The molecular ions (M^+) of the enzyme substrate (370 m/z) and product (386 m/z) were selected for secondary fragmentation. MRM optimization was then employed to maximize transition intensity and sensitivity for each fragment allowing for

Scheme 4. Synthesis of (*Z/E*)-4-Amino-2-methylbut-2-en-1-ol hydrochloride (6, 6')

quantitation of product ions. The optimized MRM method was used to verify both substrate and product by direct injection of enzymatic assays. These results were compared to direct injection of synthetic standards.

Synthesis of Nucleoside Analogues. Three ribonucleosides were prepared as shown in Scheme 2. (See Supporting Information for detailed experimental procedures.) Briefly, 2-methylthio-*N*⁶-isopentenyl-adenosine (**5a**), ms²i⁶A₃₇, was prepared from commercially available thioxanthine. Selective S-methylation of thioxanthine was achieved by adding dimethyl sulfate while maintaining a temperature below 30 °C.⁴² The corresponding product was then chlorinated by addition of phosphorus oxychloride and *N,N*-dimethylaniline, producing 2-methylthio-*N*⁶-chloropurine (**1a**).⁴² Isopentenylamine hydrochloride (**2**) was synthesized via Gabriel synthesis,^{43,44} and conveniently isolated as the HCl salt.⁴⁵ Isopentenylamine hydrochloride (**2**) was added by chemoselective nucleophilic aromatic substitution at the C6-position.^{46,47} Freshly prepared 1,2,3,5-tetra-*O*-acetyl-D-ribofuranose (**4**)⁴⁸ was then coupled to the purine via modified Vorbrüggen coupling^{49,50} and subsequently deprotected by saponification to provide the desired product, **5a**. Analogues **5b–c** were synthesized in a similar manner from commercially available xanthine, which was converted to 2,6-dichloropurine.⁵¹ 2-Chloro-*N*⁶-isopentenyl-purine was accessed by chemoselective nucleophilic aromatic substitution at the C6-position.⁵² *N*⁶-Isopentenyl-adenosine (**5b**) was prepared by utilizing Grignard conditions for hydrodehalogenation at the C2-position (**3c** to **3b**).⁵³

Hydroxylated **8a–c**, expected MiaE oxidation products, were constructed as illustrated in Scheme 3, using (*E*)-4-hydroxyisopentenylamine hydrochloride (**6**) in place of amine **2**. *N*-Boc glycine methyl ester (**9**) could be converted to aldehyde (**10**) directly by reduction with diisobutylaluminumhydride (DIBAL) or by conversion to *N*-Boc ethanolamine then selective oxidation (not shown).⁵⁴ Aldehyde **10** was converted to either (*Z*)- (**11**) or (*E*)-4-amino-2-methylbut-2-enoic acid ethyl ester-4-carboxylic acid-*tert*-butyl ester (**12**) by Horner-Wadsworth-Emmons olefination. For clarity, *Z*-stereoisomers in synthetic schemes are designated by a prime ('). *E/Z* selectivity was employed by altering the base from DBU to *n*-BuLi, and adjusting the temperature of the reaction, allowing for the production of the kinetic *Z*-diastereomer in a 4:1 ratio. DIBAL or lithium aluminum hydride treatment reduced the ester to the alcohol, which was then *N*-Boc deprotection with hydrochloric acid, to afford (*Z*)-(**6'**) or (*E*)-4-hydroxyisopentenylamine hydrochloride (**6**), respectively (Scheme 4). For further synthetic details, refer to Supporting Information.

Steady-State Kinetic Assays. Hydroxylation of substrate surrogates **5a–c** by MiaE were assayed utilizing the peroxide-shunt pathway^{21,22} frequently observed with heme and nonheme iron oxygenase enzymes. The standard assay conditions included the addition of 25 μL of 400 μM purified MiaE, 25 μL of 23 mM substrate [3:2 DMSO:HEPES buffer (20 mM HEPES, 50 mM sodium chloride buffer, pH 8)], 25 μL of 120 mM hydrogen peroxide in HEPES buffer, and 25 μL HEPES buffer to bring the final volume to 100 μL. The reactions were carried out at 27 °C, and followed for up to one hour. At selected time points, the sample was heat inactivated at 95 °C for 1 min, and then cooled to 0 °C in an ice bath. The sample was centrifuged at 14 000 rpm for 15 min, transferred into a Costar Spin-X centrifuge tube filter, and filtered at 11 500 rpm for 3 min. For samples analyzed via HILIC (Fruic-N) HPLC method, 100 μL of eluent was added prior to initial centrifugation. Since peak distortion can be caused by variable aqueous content in HILIC separations,⁵⁵ an additional 1300 μL of eluent was added to each sample, resulting in an overall 15-fold dilution in the mobile phase. The results were then analyzed by thin layer chromatography (TLC), HPLC (273 nm), and LC-MS/MS in MRM mode as described previously.

RESULTS

Purification. Recombinant MiaE from *Salmonella typhimurium* was purified and assayed for Fe-content as described in Materials and Methods. As indicated by Figure 1, the IPTG-inducible MBP-MiaE fusion protein exhibits an apparent molecular weight of ~70 kDa as observed by SDS PAGE. Overnight cleavage with TEV protease resulted in two protein bands ~40 kDa and ~25 kDa, for MBP and MiaE, respectively (Figure 1, lane 6). Following buffer exchange by dialysis, MiaE and MBP were easily resolved by a secondary DEAE anion exchange column as shown in (Figure 1, lane 7). The molecular weight of MiaE observed by SDS PAGE (~25 kDa) is slightly lower than the value expected based on its amino acid sequence (29 kDa).¹¹ Therefore, both size exclusion chromatography and analytical ultracentrifugation were utilized to confirm that purified MiaE has a monomeric (α) protein configuration in solution. Indeed, in all samples analyzed, no detectable mass action effect were observed and the predicted molecular weight (29 360 Da) was consistent with the monomeric molecular weight of MiaE. These findings were within 1% of the molecular weight calculated from the amino acid sequence (29 013.5 Da) and are consistent with those previously published for this enzyme.¹¹

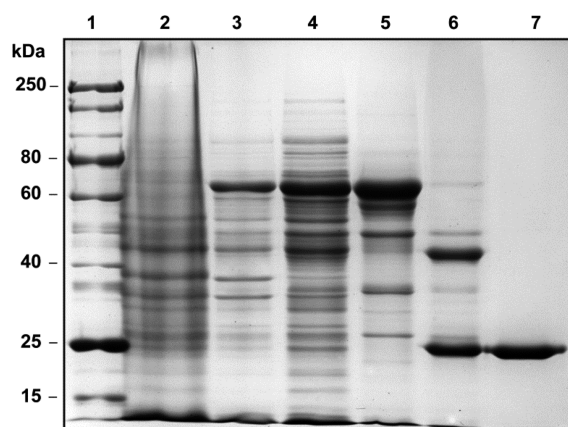


Figure 1. SDS PAGE (12%) of sequential MiaE purification steps. Lane: 1, protein markers; 2, pre-IPTG induced; 3, post-IPTG induced; 4, cell free extract; 5, MBP-MiaE fusion isolated from DEAE AX column A; 6, TEV cleaved fusion protein; 7, isolated MiaE following anion exchange DEAE column B.

The stoichiometry of iron per MiaE protein was determined by TPTZ, Bradford assay, and UV–visible spectroscopy as described previously.³² In multiple preparations of MiaE, the total iron quantification was measured at 2.1 ± 0.4 iron per MiaE protein. Moreover, the amount of Fe(III) observed by X-band EPR spectroscopy at 10 K (data not shown) did not exceed ~6% of the total iron within the sample; thus, adventitious iron does not appear to be present in significant amounts within batches of purified MiaE.

UV–visible and EPR Spectroscopy. As illustrated in Figure 2A, the as-isolated (diferric) MiaE has a yellow color due to its UV–visible absorption features ranging from ~320 to 400 nm. Such Fe-associated ligand to metal charge transfer bands are typical of nonheme diiron enzyme containing a bridging μ -oxo ligand.^{11,28} The molar extinction coefficient for this MiaE diferric cluster was determined by two independent methods.

First, the absorbance at 370 nm was measured by UV–visible spectroscopy for multiple samples of purified MiaE. Iron content was determined for each sample (as described above) and the concentration of diferric sites was taken as half the total ferric iron concentration. On the basis of this analysis, the molar extinction coefficient at 370 nm for the diferric cluster within resting MiaE was determined to be $\epsilon_{(370)} = 4900 \pm 600 \text{ M}^{-1} \text{ cm}^{-1}$ ($n = 5$ replicates).

However, this determination assumes that all optical absorbance at 370 nm is solely attributed to the oxidized enzyme. Moreover, it assumes that all of the iron present in the sample is bound within the active site of MiaE, and thus does not account for the presence of adventitiously bound iron (6% as determined above). Since the absorbance at 370 nm is attributed to diferric cluster within MiaE and not adventitious iron, UV–visible spectroscopy can be used to analytically observe the fraction of oxidized diferric enzyme present during reductive titrations with a calibrated solution of sodium dithionite mediated by methyl viologen. Although, reduced methyl viologen exhibits several absorption features in the visible region, at the concentrations of mediator utilized in these experiments ($\sim 0.4 \mu\text{M}$) its absorbance ($A \sim 0.005$) is negligible and thus can be ignored. Additionally, as shown in Supporting Information (Figure S4), due to the proximity of the large protein derived peak at 280 nm, the baseline of the reduced MiaE spectra at 370 nm is nonzero, and thus must be corrected for in the determination of the molar extinction coefficient for the resting enzyme.

In a typical experiment, a stock solution of sodium dithionite was prepared and calibrated by titration with potassium ferricyanide as described in Materials and Methods and Supporting Information (Figure S3). Aliquots ($\sim 4 \mu\text{L}$) of calibrated dithionite solution (5.9 mM reducing equivalents) were added under constant mixing to 1.4 mL of anaerobic MiaE ($40 \mu\text{M}$) using a $10 \mu\text{L}$ Hamilton gastight syringe. Following each addition of reductant, the UV–visible spectrum was monitored for ~ 5 min to ensure that reduction had gone to

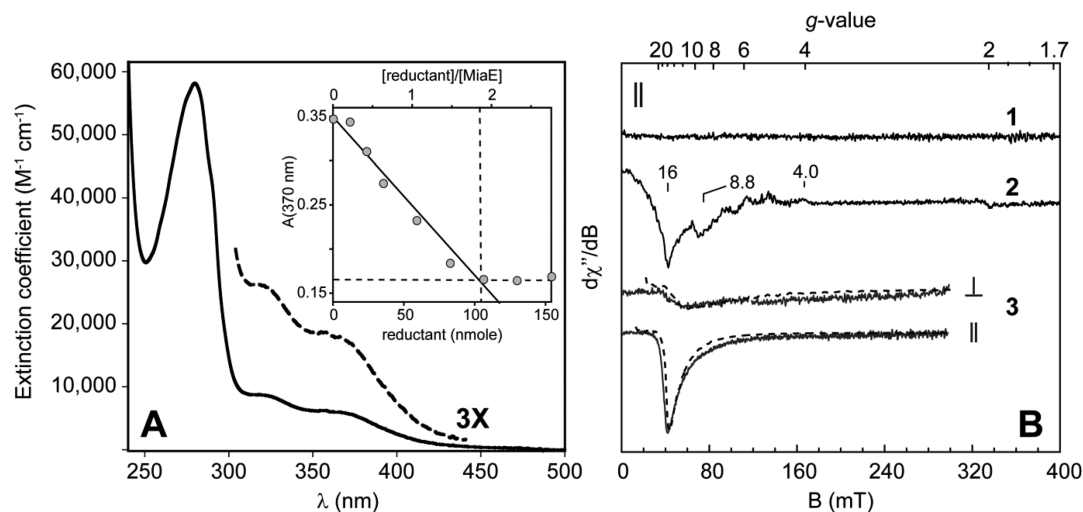


Figure 2. UV–visible and EPR spectra of MiaE. A. Optical spectra of as-isolated diferric MiaE (Inset: absorbance at 370 nm upon titration with sodium dithionite and catalytic methyl viologen). B. 4.2 K perpendicular (\perp) and parallel mode (\parallel) X-band EPR spectra of pMIAE80K expression in BL21(DE3) cell suspension ($\sim 1 \text{ mg}/\mu\text{L}$). (1) preinduction (\parallel); (2) 4 h IPTG induction (\parallel); (3) perpendicular and parallel mode X-band EPR of purified MiaE (0.25 mM) chemically reduced with excess sodium dithionite and catalytic methyl viologen. Spectroscopic simulations overlaid on spectra shown in dashed lines. EPR instrumental parameters: microwave frequency, (\perp) 9.644 GHz, (\parallel) 9.375 GHz; microwave power, (1 and 2) 6.3 mW, (3) 63 mW (\perp) and 0.63 mW (\parallel); modulation amplitude, 0.92 mT; temperature, 4.2 K. $S = 4$, $g_x = g_y = g_z = 2$; $D = 1.0 \text{ cm}^{-1}$; $E/D = 0.09$; $\sigma_D = 0.10 \text{ cm}^{-1}$; $\sigma_{E/D} = 0.05$; $\sigma_B = 1.4 \text{ mT}$; $[S] = 0.11 \text{ mM}$ (43% of theoretical).

completion prior to adding more dithionite solution. As observed in the inset of Figure 2A, addition of sodium dithionite solution results in a steady decrease in the absorbance at 370 nm consistent with reduction of the diferric cluster. From the inflection point at which the absorbance at 370 nm no longer decreases with added reductant, the total concentration of MiaE diferric clusters can be obtained. For clarity, this inflection point is designated by the crossing of the dashed lines within the inset of Figure 2A.

Based on the assumption that 2 reducing equivalents are required for each diferric cluster, the molar extinction coefficient at 370 nm can be determined for the oxidized enzyme from the difference in the absorbance observed between the oxidized and reduced MiaE ($A \sim 0.188$ AU) and dividing this value by half the moles of reductant added (53 nmol) [$\epsilon_{(370)} = 4970 \text{ M}^{-1} \text{ cm}^{-1}$]. The average value obtained over ($n = 3$) replicate measurements was $\epsilon_{(370)} = 5100 \pm 700 \text{ M}^{-1} \text{ cm}^{-1}$ (mean \pm std. dev.). From the reducing equivalents added and the protein content within the each sample, an average stoichiometry of 1.9 ± 0.1 mol of Fe is observed per MiaE protein. This value is quite similar to reported ϵ -values for other nonheme diiron enzymes exhibiting a bridging μ -oxo ligand.^{56–58}

Of particular note, the intensity of the 370 nm Fe-associated features demonstrates a clear pH dependence within the range of 7.5 to 8.5. As illustrated in Supporting Information (Figure S5), at fixed protein concentration, the relative absorbance at 370 nm shows a maximal value at pH ~ 8.4 ($\sim 35\%$ higher as compared to pH 7.6) and an apparent midpoint at pH ~ 8.1 . Similar behavior has been reported for nonheme diiron enzymes where the μ -oxo bridging ligand separating the diiron cluster is in equilibrium with the protonated μ -hydroxo species.^{11,59,60} As enzymes containing a μ -hydroxy bridged diiron cluster typically lack Fe-associated absorption features,⁶¹ the molar extinction coefficient determined above is likely underestimated. Therefore, additional experiments involving Mössbauer spectroscopy are necessary to more accurately refine these measurements.

In parallel mode X-band EPR spectroscopy, many nonheme diiron enzymes exhibit a low field signal with a distinct valley at $g \sim 16$ in the fully reduced, diferrous oxidation state.^{62–65} Among nonheme diiron enzymes, this feature is attributed to the weak ferromagnetic exchange coupling between two high-spin ferrous sites ($S_1 = S_2 = 2$), resulting in a ground state $S = 4$ spin-manifold. In nonheme diiron model complexes and bacterial multicomponent monooxygenases (MMOH and T4MOH), the observed $g \sim 16$ signal can be remarkably intense and observed at very low concentrations ($\geq 30 \mu\text{M}$ at 4 K). This is also the case for reduced MiaE. As illustrated in Figure 2B, a $g \sim 16$ signal (spectra 2) can be observed within a suspension of BL21(DE3) *E. coli* cells following 4 h IPTG-induction. In these experiments, samples were prepared by adding ~ 0.3 g cell paste in 0.3 mL 50 mM potassium phosphate, 20% glycerol, pH 7. The suspension was then transferred to an EPR tube and frozen in liquid N_2 . The additional signal observed at $g \sim 8.8$ is consistent with high-spin ferrous iron.⁶⁴ For comparison, the parallel mode EPR spectra of BL21(DE3) *E. coli* cells prior to induction and the purified fully reduced MiaE are shown in spectra 1 and 3, respectively. The temperature dependence of the MiaE $g \sim 16$ signal deviates from Curie law behavior in that the temperature-normalized signal intensity ($S \times T$) decreases with increasing temperature. Maximal intensity for this signal is observed at 4.2

K and completely vanishes by 25 K (data not shown). Therefore, this transition must originate from a ground doublet within the lowest-lying spin-manifold of a non-Kramers system. The EPR resonance condition for a non-Kramers doublet is given by $(h\nu)^2 = \Delta^2 + (g\tilde{B})^2$, where Δ represents the zero-field splitting separating the quasi-degenerate EPR active doublet and \tilde{g} is the angle dependent effective g -value.^{62,66}

Provided $\Delta < 0.3 \text{ cm}^{-1}$ (X-band $h\nu \sim 0.3 \text{ cm}^{-1}$), simulations of the reduced diiron cluster can be generated with the assumption that ferromagnetic exchange coupling constant (J) is comparable or larger in magnitude than the zero field splitting term (D) (i.e., $|J| \geq D$). Under such constraints, the $S = 4$ spin-Hamiltonian (eq 1) can be utilized to calculate correct EPR transition probabilities, and thus sample concentrations can be calculated.^{60,62,66} Comparison of the simulated diferrous site concentration to the expected value determined by UV-visible spectroscopy can then be used as an additional means to validate EPR spectroscopic simulations. Using this procedure, X-band EPR spectral simulations (dashed lines) were calculated for both perpendicular and parallel mode and overlaid on the observed spectra. As observed in Figure 2B (spectra 3), both X-band perpendicular and parallel mode EPR spectra can be simulated for $D = 1.0 \text{ cm}^{-1}$, $E/D = 0.087$, and $g_x = g_y = g_z = 2.0$. Distribution in the value of E/D ($\sigma_{E/D} = 0.05$) provides good agreement to spectral data in both field polarization modes. The spin concentration determined from EPR simulations [S] = $108 \mu\text{M}$ (43% of theoretical value). The observed deviation between the concentration theoretically calculated by EPR spectroscopic simulation and that expected on the basis of UV-visible spectroscopy suggests that the simplified assumptions made in simulations of the reduced diiron center may not be fully justified.

The fact that the $g \sim 16$ signal can be observed during *in vivo* expression demonstrates that a significant fraction of expressed MiaE is reduced at physiologically relevant potentials. Collectively, the observed Fe-stoichiometry [2 Fe per MiaE α -monomer], Fe-associated LMCT bands for the diferric enzyme, and the parallel mode $g \sim 16$ EPR signal for the fully reduced MiaE clearly demonstrates the integrity of the nonheme diiron site within the recombinantly expressed MiaE.

In Vivo MiaE Activity. The activity of recombinant MiaE was confirmed in whole cell assays following a similar protocol as described previously.^{11,17} In these experiments, *E. coli* BL21(DE3) was transformed with either the 'untagged MiaE' or TEV vector (pMIAEK and pMHT Δ 238, respectively) for comparison of total nucleoside extracts. Samples were prepared as described in Materials and Methods. Both pMIAEK (untagged MiaE) and pMHT Δ 238 (TEV) vectors have the same Promega flexi-vector backbone and antibiotic resistance, therefore RNA extracts isolated from cells transformed with pMHT Δ 238 offer a reasonable baseline for nucleoside distribution in the absence of MiaE. The chromatograms shown in Figure 3 represents the nucleosides obtained from *E. coli* post-IPTG induction (4 h) of TEV (A) and untagged MiaE (B). Of particular note are the peaks observed at 67 and 81 min designated by (open circle and circle, respectively). The peak at 81 min (circle) is observed in all nucleoside samples collected for pre- and post-IPTG induction of pMIAEK, as well as cells transformed with pMHT Δ 238. On the basis of its retention time, UV-visible spectra, and coelution with synthetic standards (trace C; 5a, β -epimer), this peak is assigned to $\text{ms}^2\text{i}^6\text{A}$. Alternatively, the 67 min peak (open circle) is only observed following IPTG-induction of pMIAEK, and coelutes

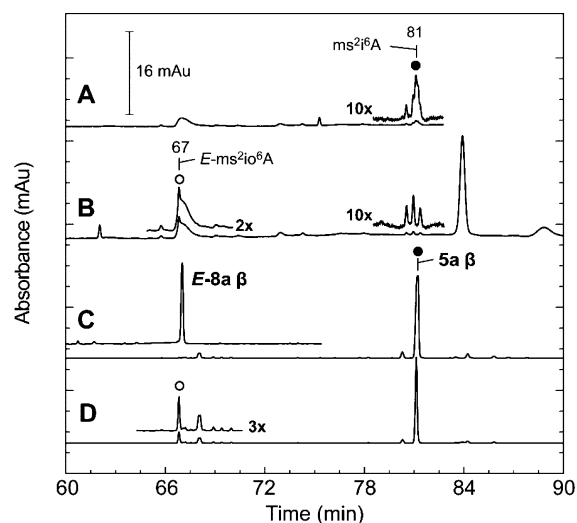


Figure 3. Reverse phase C18 HPLC chromatogram of hydrolyzed tRNA nucleosides extracted from IPTG-induced *E. coli* BL21(DE3) transformed with (A) pMHTΔ238 and (B) pMIAEK. Assignment of (*E*)- ms^2i^6A (67 min) and ms^2i^6A (81 min) β -epimers were confirmed by comparison of retention times and UV–visible spectra to synthetic standards (C). For clarity, a selected time point (30 min) is shown in trace D for the MiaE peroxide-shunt catalyzed hydroxylation of 5a.

with *E*-8a, β -epimer. On the basis of these experiments, it is clear that recombinant MiaE is catalytically active in whole cells. Moreover, as illustrated in Figure 3 (trace D), the 5a-hydroxylated product generated by MiaE peroxide-shunt nicely overlaps with the *E*- ms^2i^6A -product observed in whole cell assays. Thus, the native stereoselectivity of MiaE appears unperturbed in peroxide-shunt assays.

Catalase Activity. Many nonheme diiron oxygenase enzymes exhibit limited catalase activity as a result of the peroxide-shunt pathway.³⁶ While this activity is several orders of magnitude less than that of a ‘true’ catalase enzyme, this

assay can be diagnostic of the specific activity of purified MiaE in the absence of the native ($ms^2i^6A_{37}$) substrate. In these experiments, a standard Clarke-type oxygen electrode was used to monitor the amount and initial rate of O_2 -evolved upon addition of as-isolated MiaE to a buffered solution (20 mM HEPES, 100 mM NaCl, and pH 8) containing hydrogen peroxide. The volume of each reaction was fixed at 1.5 mL with a final MiaE Fe_2 -site concentration of 5 μ M. For analysis, initial rates were normalized for enzyme concentration ($v_0/[E]$) and H_2O_2 concentrations were varied between 15 and 80 μ M at 25 °C. As shown in Supporting Information (Figure S6), full enzymatic saturation kinetics was not observed within the range of H_2O_2 utilized (0–80 μ M). However, from the linear portion of the curve, the pseudo-second-order rate constant was determined ($k_{obs} \sim 1480 M^{-1}\cdot s^{-1}$). The stoichiometry of H_2O_2 consumed per O_2 generated was determined by addition of (120 μ M) H_2O_2 to a buffered solution containing 10 μ M MiaE. Upon completion of the reaction (2 min), the O_2 concentration within the solution increased by 62 μ M. In multiple replicates, formation of 1.1 ± 0.2 ($n = 5$) mol of O_2 is observed upon addition of 2 mol H_2O_2 .

Hydroxylation of Substrate-Surrogates by Peroxide Shunt.

Nonheme diiron monooxygenases often exhibit a peroxide shunt pathway, which can be exploited to bypass the native electron transport chain necessary for *in vivo* catalysis. For initial screening of synthetic substrate-surrogates, TLC was used to qualitatively observe the formation of hydroxylated products and decay of the starting material. Using this method, preliminary assays were performed to determine if the $ms^2i^6A_{37}$ substrate-analogues [isopentenylamine hydrochloride (2), 2-chloro- N^6 -isopentenyl-purine (3c), 2-chloro- N^6 -isopentenyl-adenosine (5c)] were hydroxylated by MiaE in the presence of hydrogen peroxide (20 mM). As a control, duplicate samples were prepared in the absence of MiaE to verify that the observed products were not the result of direct oxidation by H_2O_2 . An additional control sample was prepared using heat-denatured MiaE. In these preliminary assays, complex 2 showed

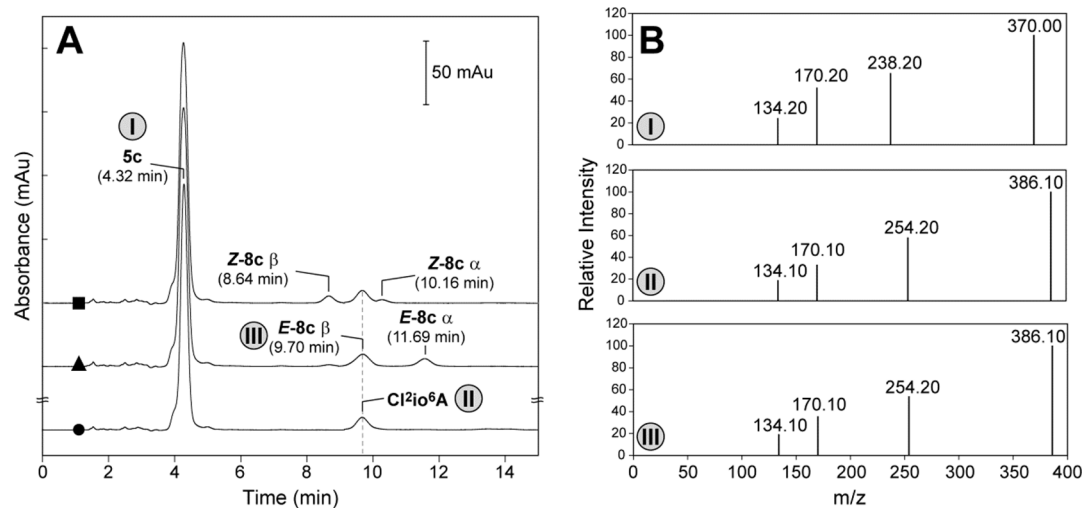


Figure 4. (A) HILIC chromatogram of product formation, along with spike analysis to verify structure and stereochemistry. The bottom chromatogram represents the *in vitro* enzymatic assay. The middle chromatogram represents the spike addition of *E*-8c diastereomeric mixture. The top chromatogram represents the spike addition of *Z*-8c diastereomeric mixture. The product of the MiaE transformation correlates with the β -epimer of the *E*-8c stereoisomer as indicated by overlapping retention time (dashed line) and an increase in the *E*-8c β peak area upon spike addition. (B) LC-MS/MS spectra of MRM transitions of designated product ions. The top panel (I) represents the substrate 5c, while the middle panel (II) represents the enzymatic product (both obtained by direct injection of *in vitro* assay). The bottom panel (III) represents the synthetic product standard *E*-8c.

no obvious sign of decay with MiaE over the course of the experiment (1 h), and the limited solubility of complex 3c made analysis impossible. However, complex 5c showed an obvious decay with time and concomitant formation of a new spot (Supporting Information, Figure S1). Moreover, the R_f -value (0.18) for this new spot correlates with that of the synthesized 2-chloro- N^6 -((*E*)-4-hydroxyisopentenyl)-adenosine (8c). Preparatory TLC and high resolution mass spectral analysis indicated a mass equivalent to expected product [HRMS (EI) found 386.1231 m/z ; calculated 386.1153 Da]. No products were observed in control samples within the time scale of these reactions.

To confirm that the MiaE hydroxylated product corresponds to the synthetic (8c) product, spike assays were performed in which the synthetic product was added into samples taken from the *in vitro* MiaE assay. As with the experiments described above, control experiments performed in the absence of MiaE or utilizing heat-denatured MiaE showed no detectable peaks corresponding to 8c formation. Figure 4A (bottom, circle) shows a representative chromatogram obtained from the MiaE assay. The larger peak observed at a retention time of 4.32 min corresponds to the enantiomerically pure β -substrate (5c) whereas the MiaE hydroxylated product is observed at 9.70 min. For clarity, these peaks are designated I and II, respectively.

The two remaining chromatograms in Figure 4A represent the same MiaE assay sample in which a diastereomeric mixture of α/β E-8c (middle, triangle) and Z-8c (top, square) was added to the sample. In addition to the peak corresponding to substrate (5c), two additional peaks are observed in the middle (triangle) chromatogram at 9.70 and 11.69 min corresponding to the β - and α -diastereomers of E-8c, respectively. The peak corresponding to the β -epimer of the synthetic E-8c is designated by III. For comparison, addition of the diastereomeric mixture of Z-8c (α -epimer, 10.16; and β -epimer, 8.64 min) is shown in the top (square) chromatogram of Figure 4A. Given that an enantiomerically pure substrate was utilized in enzymatic reactions, the observed increase in peak area of the E-8c β -enantiomer with spike addition, along with the overlapping retention time (dashed line), strongly supports assignment of the MiaE product (β -8c) and *E*-stereochemistry. Representative chromatograms of product standards E-8c and Z-8c, along with selected enzymatic assays utilizing substrate 5c, are provided in Supporting Information Figure S2. For all substrates assayed (5a-c), no more than 3% of the hydroxylated Z-product was ever observed within the time scale of peroxide-shunt assays.

As final verification of MiaE hydroxylated product, LC-MS/MS was performed on the peaks designated I, II, and III using MRM transitions of respective product ions as described in Materials and Methods. The top panel (I) Figure 4B represents the substrate 5c mass spectrum (370 m/z molecular ion), whereas the middle and bottom panels represent the mass spectrum obtained from the enzymatic product (II) and synthetic E-8c standard (III), respectively. The molecular ion (M^+) is observed in each, with an increase of 16 (hydroxyl ion) in both the enzymatic product (II) and product standard (III) [$M^+ = 386.1$ m/z]. The m/z 238 of 5c, along with the m/z 254 of enzymatic product and E-8c, is the result of the ribose cleavage and thus also exhibit an increase in mass by 16 m/z consistent with hydroxylation. The m/z 170 fragment is a result of isopentenyl cleavage, followed by m/z 134 representing a loss of HCl. In light of the matching fragmentation patterns and

relative intensities obtained for MiaE product (II) and the synthetic product standard E-8c (III), the increase in molecular ion by 16 m/z , and overlapping retention times obtained in spike assays described above, it appears that the MiaE hydroxylated product generated by peroxide shunt assays can be attributed to E-Cl²io⁶A.

Optimal concentration of H₂O₂ for MiaE peroxide-shunt assays was determined by the method of isolation. In these experiments, the concentration of substrate 5c was fixed (5.8 mM) while H₂O₂ concentrations were varied from 5 to 50 mM. The reaction was initiated by addition of 100 μ M MiaE (Fe₂-sites) at 27 °C. At selected time points (1–9 min), sample aliquots were removed for heat inactivation (95 °C for 1 min) and spin-filtered to remove denatured protein as described in Materials and Methods. Figure 5 shows the initial rate ($v_0/[E]$)

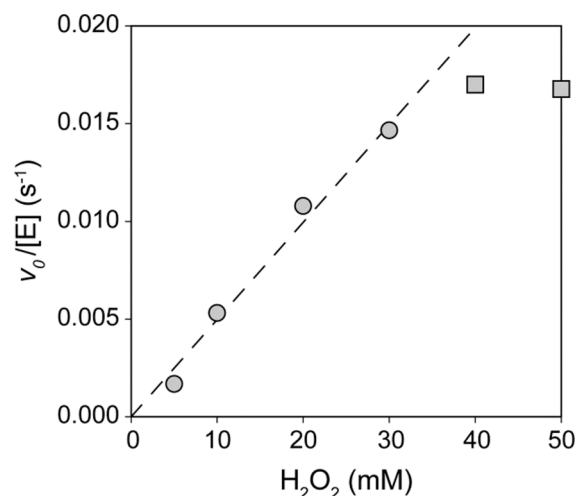


Figure 5. Enzyme normalized initial rate ($v_0/[E]$) of product formation (Cl²io⁶A) with increasing H₂O₂ concentration. The pseudo-second-order rate constant was determined by linear regression (dashed line; $k_{obs} = 5.0$ M⁻¹·s⁻¹). Assay conditions: 100 μ M MiaE, 5.8 mM 5c, 25 mM HEPES, 50 mM NaCl, pH 8, H₂O₂ (5–50 mM).

of product (Cl²io⁶A) produced as a function of initial hydrogen peroxide concentration. As with the catalase assays (Supporting Information Figure S6), full saturation of MiaE is never observed within the concentration range utilized for these experiments (1–50 mM). Since visible signs of protein denaturation were observed at H₂O₂ concentrations ~40 mM, the decrease in $v_0/[E]$ observed is likely due to enzymatic degradation and not substrate saturation. Therefore, 30 mM H₂O₂ was used for subsequent assays.

As illustrated in Figure 6, the rate of substrate (5c) degradation (circle) at 30 mM H₂O₂ is kinetically matched to the rate of product (Cl²io⁶A) formation (square). Moreover, in the absence of MiaE (Figure 6, triangle), no decay of 5c (or formation of Cl²io⁶A) can be observed within the time scale of these experiments. This observation indicates that H₂O₂ cannot (by itself) specifically oxidize the substrate and that product decay and substrate formation are coupled (1:1 stoichiometry) within the MiaE peroxide-shunt assay. By contrast, given the low-level catalase activity of MiaE it is unlikely that the stoichiometry of H₂O₂ consumed per mole of product is closely matched.

Substrate-Analogue Study. MiaE specificity for synthetic substrate-analogues (5a-c) was determined using the method of

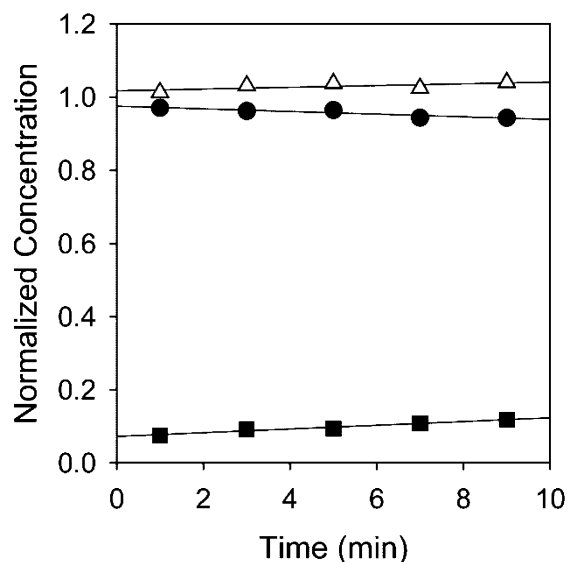


Figure 6. Stoichiometric coupling of **5c** decay (●) and $\text{Cl}^2\text{io}^6\text{A}$ formation (■) in Mia peroxide shunt pathway. Within error, the rates of substrate decay and product formation are kinetically matched (0.01 min^{-1}). The control of **5c** in the absence of MiaE (Δ , H_2O_2 only) is overlaid for comparison. Assay conditions: $100 \mu\text{M}$ MiaE, 5.8 mM **5c**, 30 mM H_2O_2 , 25 mM HEPES, 50 mM NaCl, 15–20% DMSO (v/v), pH 8.

isolation as described above. However, in these experiments the hydrogen peroxide concentration was fixed at 30 mM while varying the concentration of nucleosides (**5a-c**). Given the low solubility of synthetic nucleosides (**5b** in particular), dimethyl sulfoxide (DMSO) was added to the enzymatic reactions to increase the upper limit of substrate concentration. Control reactions containing up to 20% (v/v) DMSO showed no effect on the rate of $\text{Cl}^2\text{io}^6\text{A}$ formation by MiaE peroxide shunt. Only DMSO concentrations exceeding 25% (v/v) demonstrated a noticeable decrease in the rate of peroxide-shunt product hydrolysis. Therefore, all of the enzymatic assays described below were carried out in the standard HEPES buffer with 20% DMSO (v/v).

For each assay, the concentration of substrate analogue was varied from 0.5 to 4 mM (depending on solubility) at fixed H_2O_2 concentration (30 mM). As previously stated, reactions were initiated by addition of $100 \mu\text{M}$ MiaE (Fe_2 -sites) at 27°C and sample aliquots were taken at times ranging from 1 to 9 min. HPLC sample preparation was carried out as described previously. Figure 7 shows the initial rate of product formation ($\text{ms}^2\text{io}^6\text{A}$, io^6A , and $\text{Cl}^2\text{io}^6\text{A}$) plotted against the starting concentration of each substrate (**5a-c**) analogue. Each substrate saturation kinetic experiment was performed in duplicate. For clarity, only the error observed in the initial rate of **8c** formation is indicated in Figure 7.

As expected, the initial rate of product formation increases to a maximal value with increasing substrate concentration. However, at elevated concentrations, the rate of product formation decreases significantly for each nucleoside, suggesting something analogous to substrate-inhibition or decreased enzyme activity near the solubility limit of the synthetic nucleosides (**5a-c**). Given the complexity of this system, development of a full kinetic model is complicated and prone to overinterpretation. However, as with H_2O_2 saturation experiments, comparison of initial rates within the linear range (1–3 mM) can be made. Shown in Figure 7 is a plot of

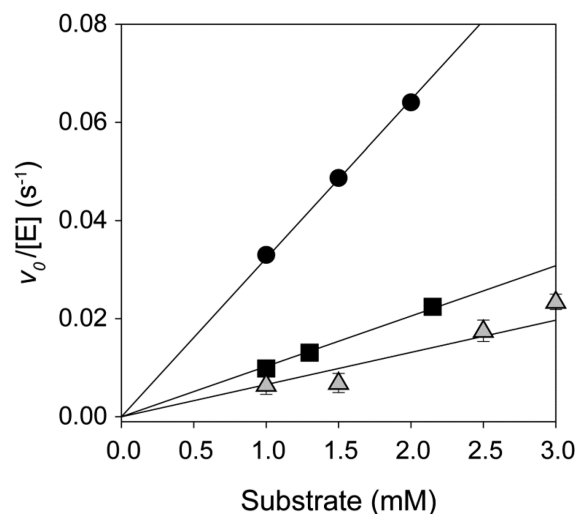


Figure 7. Enzyme normalized initial rate ($v_0/[\text{E}]$) of product ($\text{ms}^2\text{io}^6\text{A}$, io^6A , and $\text{Cl}^2\text{io}^6\text{A}$) formation with increasing substrate concentration. The pseudo-second-order rate constant for **5a** (●, -SMe), **5b** (■, -H), and **5c** (Δ , -Cl) was determined by linear regression to be 32.3 , 10.3 , and $6.6 \text{ M}^{-1}\cdot\text{s}^{-1}$, respectively. Assay conditions: $100 \mu\text{M}$ MiaE, 30 mM H_2O_2 , 25 mM HEPES, 50 mM NaCl, 15–20% DMSO (v/v), pH 8, **5a-c** (1–3 mM).

the initial rate of product formation (**8a-c**) versus substrate concentration. As in H_2O_2 -saturation experiments (Figure 5), all initial rates are normalized for enzyme concentration ($v_0/[\text{E}]$). At fixed H_2O_2 concentration (30 mM), the slope of the line can be interpreted as the pseudo-second-order rate constant (approximately k_{cat}/K_m). On the basis of this interpretation, the rate of MiaE catalyzed H_2O_2 -shunt hydroxylation for **5a** (2-SMe), **5b** (2-H), and **5c** (2-Cl) can be estimated as 32.3 , 10.3 , and $6.6 \text{ M}^{-1}\cdot\text{s}^{-1}$, respectively.

DISCUSSION

Nucleoside Substrate Synthesis. A divergent synthetic strategy led to the preparation of three nucleoside mimics with varied functionalization at the C2-position, 2-SMe ($\text{ms}^2\text{io}^6\text{A}$), 2-H (io^6A), and 2-Cl ($\text{Cl}^2\text{io}^6\text{A}$). Additionally, two diastereomers of each expected oxidized product were prepared, giving rise to six additional nucleosides (E/Z - $\text{ms}^2\text{io}^6\text{A}$, (E/Z)- io^6A , and (E/Z)- $\text{Cl}^2\text{io}^6\text{A}$). The Vorbrüggen coupling of the purine derivatives to tetraacetylribose provided a metal-free preparation, and resulted in comparable yields.^{67–69} The nucleosides were synthesized in eleven or fewer steps from commercially available materials and with 10–15% overall yield. As discussed below, the synthesis of these nucleosides allowed for the stereochemical determination of the MiaE modified product ($E\text{-ms}^2\text{io}^6\text{A}$), along with the overall effect of the C2-functionalization on rate of product formation.

Characteristics of *S. typhimurium* MiaE. In general, the physical properties of MiaE are consistent with those for other members of the nonheme diiron class of metalloenzymes. The optical features in the 320–380 nm range [$5100 \pm 700 \text{ M}^{-1} \text{ cm}^{-1}$] observed for resting MiaE are reminiscent of those observed for the μ -oxo bridged diiron clusters within other nonheme diiron metalloproteins such as the small subunit of ribonucleotide reductase (R2) [$\epsilon_{(370)} = 4350 \text{ M}^{-1} \text{ cm}^{-1}$],^{5,70} stearyl-acyl carrier protein Δ^9 -desaturase ($\Delta 9\text{D}$) [$\epsilon_{(340)} = 4200 \text{ M}^{-1} \text{ cm}^{-1}$],⁷¹ myohemerythrin (Hr) [$\epsilon_{(330)} = 6500 \text{ M}^{-1} \text{ cm}^{-1}$],⁷² and phenol hydroxylase (DpmLNO) [$\epsilon_{(350)} = 4800\text{--}$

$6000 \text{ M}^{-1} \text{ cm}^{-1}$].⁶⁰ By contrast, the oxidized diiron cluster within the hydroxylase components of bacterial methane and toluene monooxygenases (MMOH and T4MOH) are believed to have hydroxo-bridged diiron clusters and thus lack such optical features as a consequence.⁷³

The dual-mode EPR spectroscopy of reduced MiaE exhibits similar temperature-dependent signal intensity, line width, and g -values as compared to the reduced diiron sites within several other bacterial nonheme monooxygenase enzymes (DpmLNO, T4MOH, MMOH).⁶¹ As previously mentioned, spin quantitation of reduced MiaE by simulation only accounts for [0.11 mM] 44% of the total iron within the sample. This may indicate that the assumptions made in simulating the reduced diiron cluster ($|J| \geq D$) were not fully justified. However, previous Mössbauer analysis of oxidized MiaE suggests the presence of a major (54%) μ -hydroxo bridged [$\delta = 0.49 \text{ mm}\cdot\text{s}^{-1}$ $\Delta E_Q = 0.51 \text{ mm}\cdot\text{s}^{-1}$] and minor μ -oxo bridged [$\delta = 0.52 \text{ mm}\cdot\text{s}^{-1}$ $\Delta E_Q = 1.49 \text{ mm}\cdot\text{s}^{-1}$] population within the as-isolated MiaE.¹¹ Indeed, similar (μ -oxo/ μ -hydroxo) speciation has been reported from Mössbauer analysis of as-isolated and reduced $\Delta 9D$,⁵⁹ T4MOH,⁶¹ and DpmLNO.⁶⁰ In the case of reduced DpmLNO, this same (μ -oxo/ μ -hydroxo) speciation could be observed upon reduction of the resting diferric enzyme. Moreover, it was reported that only the μ -hydroxo bridged diferric cluster was EPR active.⁶⁰ Therefore, the low spin-quantitation [44% relative to the total iron] determined by EPR simulations could also be explained if reduced MiaE exhibits similar (μ -oxo/ μ -hydroxo) speciation as previously reported for the oxidized enzyme and that only the μ -hydroxo fraction is EPR active. Under these assumptions, the concentration of μ -hydroxo bridged fraction is within 10% of the simulated spin-quantitation. Given the observed pH dependence of the Fe-associated bands, it is clear that some (μ -oxo/ μ -hydroxo) speciation is present in resting MiaE. However, it is not known if this speciation remains upon reduction of the diiron center. This observation also implies that the extinction coefficient determined here for the resting diferric enzyme is likely underestimated. Investigation of the oxidized and reduced MiaE by Mössbauer spectroscopy is currently in progress to validate EPR spectroscopic simulations and refine UV-visible molar extinction coefficient determinations for this enzyme.

The monomeric (α) configuration of MiaE reported here is in agreement with previous reports.¹¹ This trait is quite unusual for nonheme diiron enzymes and, to our knowledge, has only been reported for the nonenzymatic member of this family, hemerythrin (Hr).^{72,74,75} Typically, the quaternary structures of nonheme diiron enzymes are multimeric in their native form.⁷⁶ In fact, the most common quaternary structure observed for this family of enzymes is homodimeric (α_2), whereas the most common structural motif observed among the hydroxylase components within the BMM class of nonheme diiron monooxygenases is a heterotrimeric dimer ($\alpha\beta\gamma$)₂ configuration.³¹ Interestingly, both R2 and $\Delta 9D$ have been reported to exhibit 'half-sites' reactivity, implying that the two protomers of these (α_2)-enzymes do not act independently during catalysis.^{77–80} Historically, both the structural complexity and the potential for 'half-sites' reactivity within this class of enzymes have significantly complicated the spectroscopic and mechanistic characterization of nonheme diiron enzymes. Therefore, the monomeric (α) protein configuration of MiaE represents a minimalist enzymatic structure which could potentially provide a unique point of comparison to other enzymes within this class.

MiaE Substrate Specificity Influenced by C2-Position Substitution of Nucleoside.

Initial attempts to demonstrate MiaE hydroxylation of the free purine (substrates 3a–c) were not successful given the insolubility of the base in the absence of ribose. Interestingly, within error both α - and β -epimers (5a–c) were hydroxylated at comparable rates (Table S1). This observation indicates that the ribose ring does not represent a significant enzyme–substrate point of interaction. Furthermore, since the C2-position of the nucleoside is quite distant from the point of enzymatic hydroxylation, given the observed difference in the second order reaction rate [5a (2-SMe) > 5b (2-H) > 5c (2-Cl)], it is reasonable to speculate that the nucleosides C2-substituent significantly influences the MiaE-binding affinity. For example, at a fixed substrate concentration (2.0 mM), the rate of 5a-hydroxylation is over 3-fold that of 5b-hydroxylation. Interestingly, a similar substrate preference has also been observed for $\text{ms}^2\text{i}^6\text{A}$ - and i^6A -bearing tRNA substrates.¹⁷ Therefore, it is possible that the enzymatic substrate specificity is largely a function of the nucleoside base and not due to conformational difference within the global tRNA tertiary structure.

(*E/Z*)-Stereochemistry of MiaE Hydroxylated Products (i^6A , $\text{Cl}^2\text{i}^6\text{A}$, and $\text{ms}^2\text{i}^6\text{A}$). The peroxide-shunt pathway is a common feature among nonheme diiron (and heme) oxygenase enzymes.^{21,22,38,60} The use of a peroxide-shunt simplifies the enzymatic catalysis by removing the need for an enzymatic electron-transfer pathway. However, peroxide-shunt enzymatic activities are significantly lower than native catalysis due to the competing catalase-activity, and the potential for promiscuous Fenton-type reactions leading to enzymatic degradation. Therefore, peroxide-shunt experiments should be considered diagnostic of native MiaE catalysis, but are less useful for the development of a kinetic mechanism. Additionally, relative to reactions catalyzed in the presence of their electron-transfer chain, many nonheme oxygenases exhibit decreased stereo- and chemoselectivity by peroxide-shunt.^{18,21,22} For instance, it was found that, in the presence of protein B, MMOH demonstrates a 3-fold greater selectivity in the presence of dioxygen relative to peroxide-shunt induction.¹⁸

By contrast, MiaE peroxide-shunt demonstrates a clear stereospecificity in that only the (*E*)-isomers of the hydroxylated nucleosides (8a–c) are observed. Indeed, for all substrate analyses, <3% of the (*Z*)-isomer was ever identified in peroxide-shunt reactions. Moreover, as illustrated in Figure 3, *in vivo* product formation during MiaE IPTG-induction is also consistent with the (*E*)-isomer of $\text{ms}^2\text{i}^6\text{A}$. Thus the peroxide-shunt MiaE product is consistent with native catalysis. This result was not readily anticipated given discrepancies within the literature regarding the stereochemistry of $\text{ms}^2\text{i}^6\text{A}_{37}$ isolated across phylogenetic domains. For example, early on it was reported that $\text{ms}^2\text{i}^6\text{A}_{37}$ isolated from plants exhibited (*Z*)-stereochemistry. Interestingly, in this same report it was observed that the (*E*)-isomer of i^6A_{37} could be isolated as a free-base.⁷³ Thus, suggesting the possibility of an independent pathway for cytokinin synthesis independent of MiaE. Alternatively, this observation may simply be the result of light induced *E/Z*-isomerization. Regardless, this hypothesis was never explored further. Among bacterial enzymes, it was reported that *Z*- $\text{ms}^2\text{i}^6\text{A}_{37}$ was the MiaE-product observed from various plant-associated bacteria (*Rhizobium leguminosarum*, *Agrobacterium tumefaciens*, and *Corynebacterium fascians*).⁸¹ The first instance of *E*- $\text{ms}^2\text{i}^6\text{A}_{37}$ was reported by Ajitkumar and

Cherayil for the nonplant associated γ -proteobacteria, *Azotobacter vinelandii*.¹⁵ Based on this observation it was proposed that other nonplant associated bacteria (such as *Salmonella typhimurium*) may also produce the (E) - instead of the (Z)-isomer. This is perhaps a tenuous hypothesis given only 58% identity between *S. typhimurium* and *A. vinelandii* MiaE. To our knowledge, this work represents the first direct confirmation of the *S. typhimurium* MiaE stereospecificity.

■ ASSOCIATED CONTENT

● Supporting Information

Detailed experimental procedures, ¹H and ¹³C NMR, MS data for deprotected nucleosides, and chromatography (TLC and HPLC) information. This material is available free of charge via the Internet at <http://pubs.acs.org>.

■ AUTHOR INFORMATION

Corresponding Authors

*Phone (817) 272-5245, Fax (817) 272-3808, E-mail ffoss@uta.edu.

*Phone (817) 272-9066, Fax (817) 272-3808, E-mail bspierce@uta.edu.

Funding Statement

This work was supported by start-up funds provided to B.S.P and F.W.F. Jr. from The University of Texas at Arlington, Department of Chemistry and Biochemistry. We would also like to acknowledge NSF financial support (CRIF:MU CHE-0840509) for the purchase of the JEOL ECA500 500 MHz FT-NMR spectrometers.

Notes

The authors declare no competing financial interest.

■ ACKNOWLEDGMENTS

We would like to acknowledge the UTA Shimadzu Center for Advanced Analytical Chemistry (UT-Arlington) for the use of HPLC and LC-MS/MS instrumentation utilized in this work, and the University of Wisconsin, Center for Structural Genomics members (B. G. Fox and R. Wrobel) for generously providing us with the MBP-fusion (pVP80K) and TEV expression (pMHTΔ238) vectors utilized in this work.

■ ABBREVIATIONS

MiaE, 2-methylthio-*N*⁶-isopentenyl adenosine(37)-tRNA (ms²i⁶A-tRNA) monooxygenase; tRNA, transfer ribonucleic acid; MiaA, Δ²-isopentenylpyrophosphate tRNA-adenosine transferase; MiaB, 2-methylthio-*N*⁶-isopentenyl-adenosine synthase; DMAPP, dimethylallyl pyrophosphate; SAM, S-adenosylmethionine; ms²i⁶A₃₇, 2-methylthio-*N*⁶-isopentenyl-adenosine; i⁶A₃₇, *N*⁶-isopentenyl-adenosine; Cl²i⁶A₃₇, 2-chloro-*N*⁶-isopentenyl-adenosine; ms²io⁶A₃₇, 2-methylthio-*N*⁶-(4-hydroxyisopentenyl)-adenosine; io⁶A₃₇, *N*⁶-(4-hydroxyisopentenyl)-adenosine; Cl²io⁶A₃₇, 2-chloro-*N*⁶-(4-hydroxyisopentenyl)-adenosine; ASL, anticodon stem loop; TLC, thin layer chromatography; HPLC, high-performance liquid chromatography; TEV, tobacco etch virus protease; IPTG, isopropyl β-D-1-thiogalactopyranoside; EPR, electron paramagnetic resonance

■ REFERENCES

(1) Björk, G. R., Durand, J. M., Hagervall, T. G., Leipuviene, R., Lundgren, H. K., Nilsson, K., Chen, P., Qian, Q., and Urbonavicius, J. (1999) Transfer RNA modification: influence on translational frameshifting and metabolism. *FEBS Lett.* 452, 47–51.

(2) Gustilo, E. M., Vendeix, F. A. P., and Agris, P. F. (2008) tRNA's modifications bring order to gene expression. *Curr. Opin. Microbiol.* 11, 134–140.

(3) Björk, G. R., Ericson, J. U., Gustafsson, C. E. D., Hagervall, T. G., Jonsson, Y. H., and Wikstrom, P. M. (1987) Transfer RNA Modification. *Annu. Rev. Biochem.* 56, 263–285.

(4) Persson, B. C. (1993) Modification of tRNA as a regulatory device. *Mol. Microbiol.* 8, 1011–1016.

(5) Petersson, L., Gräslund, A., Ehrenberg, A., Sjöberg, B. M., and Reichard, P. (1980) The iron center in ribonucleotide reductase from *Escherichia coli*. *J. Biol. Chem.* 255, 6706–6712.

(6) Durand, J. M., Björk, G. R., Kuwae, A., Yoshikawa, M., and Sasakawa, C. (1997) The modified nucleoside 2-methylthio-*N*⁶-isopentenyladenosine in tRNA of *Shigella flexneri* is required for expression of virulence genes. *J. Bacteriol.* 179, 5777–5782.

(7) Persson, B. C., and Björk, G. R. (1993) Isolation of the Gene (*miaE*) Encoding the Hydroxylase Involved in the Synthesis of 2-Methylthio-cis-Ribozetatin in tRNA of *Salmonella typhimurium* and Characterization of Mutants. *J. Bacteriol.* 175, 7776–7785.

(8) Moore, J. A., and Poulter, C. D. (1997) *Escherichia coli* dimethylallyl diphosphate:tRNA dimethylallyltransferase: A binding mechanism for recombinant enzyme. *Biochemistry* 36, 604–614.

(9) Arragain, S., Handelman, S. K., Forouhar, F., Wei, F.-Y., Tomizawa, K., Hunt, J. F., Douki, T., Fontecave, M., Mulliez, E., and Atta, M. (2010) Identification of Eukaryotic and Prokaryotic Methylthiotransferase for Biosynthesis of 2-Methylthio-*N*⁶-threonyl-carbamoyl-adenosine in tRNA. *J. Biol. Chem.* 285, 28425–28433.

(10) Pierrel, F., Douki, T., Fontecave, M., and Atta, M. (2004) MiaB Protein is a bifunctional radical-S-adenosylmethionine enzyme involved in thiolation and methylation of tRNA. *J. Biol. Chem.* 279, 47555–47563.

(11) Mathevon, C., Pierrel, F., Oddou, J.-L., Garcia-Serres, R., Blondin, G., Latour, J.-M., Menage, S., Gambarelli, S., Fontecave, M., and Atta, M. (2007) tRNA-modifying MiaE protein from *Salmonella typhimurium* is a nonheme diiron monooxygenase. *Proc. Natl. Acad. Sci. U. S. A.* 104, 13295–13300.

(12) Esberg, B., Leung, H.-C. E., Tsui, H.-C. T., Björk, G. R., and Winkler, M. E. (1999) Identification of the *miaB* Gene, Involved in Methylthiolation of Isopentenylated A₃₇ Derivatives in the tRNA of *Salmonella typhimurium* and *Escherichia coli*. *J. Bacteriol.* 181, 7256–7265.

(13) Buck, M., and Ames, B. N. (1984) A modified nucleotide in tRNA as a possible regulator of aerobiosis: Synthesis of cis-2-methylthioribosylzeatin in the tRNA of *Salmonella*. *Cell* 36, 523–531.

(14) Esberg, B., and Björk, G. R. (1995) The methylthio group (ms²) of *N*⁶-(4-hydroxyisopentenyl)-2-methylthioadenosine (ms²io⁶A) present next to the anticodon contributes to the decoding efficiency of the tRNA. *J. Bacteriol.* 177, 1967–1975.

(15) Ajitkumar, P., and Cherayil, J. D. (1985) Presence of 2-methylthioribosyl-trans-zeatin in *Azotobacter vinelandii* tRNA. *J. Bacteriol.* 162, 752–755.

(16) Kaminska, K. H., Baraniak, U., Boniecki, M., Nowaczyk, K., Czerwoniec, A., and Bujnicki, J. M. (2008) Structural bioinformatics analysis of enzymes involved in the biosynthesis pathway of the hypermodified nucleoside ms²io⁶A₃₇ in tRNA. *Proteins* 70, 1–18.

(17) Persson, B., Olafsson, O., Lundgren, H., Hederstedt, L., and Björk, G. (1998) The ms²io⁶A₃₇ modification of tRNA in *Salmonella typhimurium* regulates growth on Citric Acid cycle intermediates. *J. Bacteriol.* 180, 3144–3151.

(18) Feig, A. L., and Lippard, S. (1993) Reactions of non-heme iron(II) centers with dioxygen in biology and chemistry. *Chem. Rev.* 94, 759–805.

(19) Wallar, B. J., and Lipscomb, J. D. (1996) Dioxygen activation by enzymes containing binuclear non-heme iron clusters. *Chem. Rev.* 96, 2625–2658.

(20) Solomon, E. I., Decker, A., and Lehnert, N. (2003) Non-heme iron enzymes: Contrasts to heme catalysis. *Proc. Natl. Acad. Sci. U. S. A.* 100, 3589–3594.

- (21) Bailey, L. J., and Fox, B. G. (2009) Crystallographic and catalytic studies of the peroxide-shunt reaction in a diiron hydroxylase. *Biochemistry* 48, 8932–8939.
- (22) Froland, W. A., Andersson, K. K., Lee, S.-K., Liu, Y., and Lipscomb, J. D. (1992) Methane monooxygenase component B and reductase alter the regioselectivity of the hydroxylase component-catalyzed reactions. *J. Biol. Chem.* 267, 17588–17597.
- (23) Hirao, H., Li, F., Que, L., Jr., and Morokuma, K. (2011) Theoretical study of the mechanism of oxoiron(IV) formation from H₂O₂ and a nonheme iron(II) complex: O–O cleavage involving proton-coupled electron transfer. *Inorg. Chem.* 50, 6637–6648.
- (24) Murray, L. J., and Lippard, S. J. (2007) Substrate trafficking and dioxygen activation in bacterial multicomponent monooxygenases. *Acc. Chem. Res.* 40, 466–474.
- (25) Kopp, D. A., Gassner, G. T., Blazyk, J. L., and Lippard, S. J. (2001) Electron-transfer reactions of the reductase component of soluble methane monooxygenase from *Methylococcus capsulatus* (Bath). *Biochemistry* 40, 14932–14941.
- (26) Lee, D., and Lippard, S. J. (2002) Synthetic analogue of the [Fe(2)(μ-OH)(2)(μ-O(2)CR)](3+) core of soluble methane monooxygenase hydroxylase via synthesis and dioxygen reactivity of carboxylate-bridged diiron(II) complexes. *Inorg. Chem.* 41, 827–837.
- (27) Lipscomb, J. D. (1994) Biochemistry of the soluble methane monooxygenase. *Annu. Rev. Microbiol.* 48, 371–399.
- (28) Baik, M. H., Newcomb, M., Friesner, R. A., and Lippard, S. J. (2003) Mechanistic studies on the hydroxylation of methane by methane monooxygenase. *Chem. Rev.* 103, 2385–2419.
- (29) Murray, L. J., Naik, S. G., Ortillo, D. O., Garcia-Serres, R., Lee, J. K., Huynh, B. H., and Lippard, S. J. (2007) Characterization of the arene-oxidizing intermediate in ToMOH as a diiron(III) species. *J. Am. Chem. Soc.* 129, 14500–14510.
- (30) Kuo, H. H., and Mauk, A. G. (2012) Indole peroxigenase activity of indoleamine 2,3-dioxygenase. *Proc. Natl. Acad. Sci. U. S. A.* 109, 13966–13971.
- (31) Notomista, E., Lahm, A., Di Donato, A., and Tramontano, A. (2003) Evolution of bacterial and archaeal multicomponent monooxygenases. *J. Mol. Evol.* 56, 435–445.
- (32) Pierce, B., Gardner, J., Bailey, L., Brunold, T., and Fox, B. (2007) Characterization of the nitrosyl adduct of substrate-bound mouse cysteine dioxygenase by electron paramagnetic resonance: electronic structure of the active site and mechanistic implications. *Biochemistry* 46, 8569–8578.
- (33) Pierce, B. S., Elgren, T. E., and Hendrich, M. P. (2003) Mechanistic implications for the formation of the diiron cluster in ribonucleotide reductase provided by quantitative EPR spectroscopy. *J. Am. Chem. Soc.* 125, 8748–8759.
- (34) Brookes, E. H., and Demeler, B. (2007) Parsimonious regularization using genetic algorithms applied to the analysis of analytical ultracentrifugation experiments. In *Proceedings of the 9th annual conference on genetic and evolutionary computation*, pp 361–368.
- (35) Demeler, B., and Brookes, E. (2008) Monte carlo analysis of sedimentation experiments. *Colloid Polym. Sci.* 286, 129–137.
- (36) Newman, L., and Wackett, L. (1995) Purification and characterization of toluene 2-monooxygenase from *Bukholderia cepacia* G4. *Biochemistry* 34, 14066–14076.
- (37) Abragam, A., and Bleaney, B. (1970) *Electron Paramagnetic Resonance of Transition Ions*, International Series of Monographs on Physics.
- (38) Chomczynski, P., and Sacchi, N. (1987) Single-step method of RNA isolation by acid guanidinium thiocyanate-phenol-chloroform extraction. *Anal. Biochem.* 162, 156–159.
- (39) Connolly, D. M., and Winkler, M. E. (1989) Genetic and physiological relationships among the miaA Gene, 2-Methylthio-N⁶-(2-Isopentenyl)-adenosine tRNA modification, and spontaneous mutagenesis in *Escherichia coli* K-12. *J. Bacteriol.* 171, 3233–3246.
- (40) Gehrke, C. W., and Kuo, K. C. (1989) Ribonucleoside analysis by reversed-phase high-performance liquid-chromatography. *J. Chromatogr.* 471, 3–36.
- (41) Yost, R. A., and Fetterolf, D. D. (1983) Tandem mass spectrometry (MS/MS) instrumentation. *Mass Spectrom. Rev.* 2, 1–45.
- (42) Spichal, L. (2009) *Substituted 6-aminopurine derivatives as inhibitors of cytokinin oxidase/dehydrogenase and preparations containing these derivatives*, Patent Number WO2009003428.
- (43) Ragnarsson, U., and Grehn, L. (1991) Novel Gabriel reagents. *Acc. Chem. Res.* 24, 285–289.
- (44) Dumas, D. J. (1988) Total synthesis of peramine. *J. Org. Chem.* 53, 4650–4653.
- (45) Mahmud, H. (2000) Studies toward the total synthesis of martinelline and martinellie acid, Department of Chemistry and Biochemistry, Thesis, The University of Texas at Arlington, Arlington, TX.
- (46) Montgomery, J. A., and Holum, L. B. (1957) Synthesis of potential anticancer agents. III. hydrazino analogs of biologically active purines. *J. Am. Chem. Soc.* 79, 2185–2188.
- (47) Oumata, N., Ferandin, Y., Meijer, L., and Galons, H. (2009) Practical synthesis of roscovitine and CR8. *Org. Process Res. Dev.* 13, 641–644.
- (48) Liu, H., and Pinto, B. M. (2004) Efficient synthesis of the glucosidase inhibitor blintol, the selenium analogue of the naturally occurring glycosidase inhibitor salacinol. *J. Org. Chem.* 70, 753–755.
- (49) Vorbrüggen, H., and Ruh-Pohlenz, C. (2001) *Handbook of nucleoside synthesis*, John Wiley & Sons, Inc.
- (50) Ginisty, M., Gravier-Pelletier, C., and Le Merrer, Y. (2006) Chemical investigations in the synthesis of O-serinyl aminoribosides. *Tetrahedron: Asymmetry* 17, 142–150.
- (51) Sun, Z., Wang, H., Wen, K., Li, Y., and Fan, E. (2011) Solvent-free or low-solvent large-scale preparation of chloropyrimidine and analogues. *J. Org. Chem.* 76, 4149–4153.
- (52) Piguel, S., and Legraverend, M. (2007) Selective amidation of 2,6-dihalogenopurines: application to the synthesis of new 2,6,9-trisubstituted purines. *J. Org. Chem.* 72, 7026–7029.
- (53) Hara, R., Sato, K., Sun, W., and Takahashi, T. (1999) Catalytic dechlorination of aromatic chlorides using Grignard reagents in the presence of (C₂H₅)₂TiCl₂. *Chem. Commun.*, 845–846.
- (54) Powell, D. A., and Batey, R. A. (2002) Total synthesis of the alkaloids martinelline and martinellie acid via a hetero Diels-Alder multicomponent coupling reaction. *Org. Lett.* 4, 2913–2916.
- (55) Hemström, P., and Irgum, K. (2006) Hydrophilic interaction chromatography. *J. Sep. Sci.* 29, 1784–1821.
- (56) Kurtz, D. M. (1990) Oxo-bridged and hydroxo-bridged diiron complexes - a chemical perspective on a biological unit. *Chem. Rev.* 90, 585–606.
- (57) Ehrenberg, A., and Reichard, P. (1972) Electron spin resonance of the iron-containing protein B2 from ribonucleotide reductase. *J. Biol. Chem.* 247, 3485–3488.
- (58) Sanders-Loehr, J., Wheeler, W., Shiemke, A., Averill, B., and Loehr, T. (1989) Electronic and Raman spectroscopic properties of oxo-bridged dinuclear iron centers in proteins and model compounds. *J. Am. Chem. Soc.* 111, 8084–8093.
- (59) Fox, B. G., Shanklin, J., Somerville, C., and Münck, E. (1993) Stearoyl-acyl carrier protein delta-9-desaturase from *Ricinus communis* is a diiron-oxo protein. *Proc. Natl. Acad. Sci. U. S. A.* 90, 2486–2490.
- (60) Cadieux, E., Vrajamasu, V., Achim, C., Powlowski, J., and Münck, E. (2002) Biochemical, Mössbauer, and EPR studies of the diiron cluster of phenol hydroxylase from *Pseudomonas* sp. Strain CF 600. *Biochemistry* 41, 10680–10691.
- (61) Pikus, J. D., Studts, J. M., Achim, C., Kauffmann, K. E., Münck, E., Steffan, R. J., McClay, K., and Fox, B. G. (1996) Recombinant toluene-4-monooxygenase: catalytic and Mössbauer studies of the purified diiron and Rieske components of a four-protein complex. *Biochemistry* 35, 9106–9119.
- (62) Hendrich, M. P., and Debrunner, P. G. (1989) Integer-spin electron paramagnetic resonance of iron proteins. *Biophys. J.* 56, 489–506.
- (63) Paulsen, K. E., Liu, Y., Fox, B. G., Lipscomb, J. D., Münck, E., and Stankovich, M. T. (1994) Oxidation-reduction potentials of the

methane monooxygenase hydroxylase component from *Methylosinus trichosporium* OB3b. *Biochemistry* 33, 713–722.

(64) Pierce, B. S., and Hendrich Michael, P. (2005) Local and global effects of metal binding within the small subunit of ribonucleotide reductase. *J. Am. Chem. Soc.* 127, 3613–3623.

(65) Elgren, T. E., Hendrich, M. P., and Que, L., Jr. (1993) Azide binding to the diferrous clusters of the R2 protein of ribonucleotide reductase from *Escherichia coli*. *J. Am. Chem. Soc.* 115, 9291–9292.

(66) Jang, H. G., Hendrich, M. P., and Que, L. (1993) Insight into the $g \approx 16$ EPR signals of reduced diiron-oxo proteins. Structure and properties of $[\text{Fe}^{II}\text{BPMP}\{\text{O}_2\text{P}(\text{OC}_6\text{H}_5)_2\}_2]\text{Cl}$. *Inorg. Chem.* 32, 911–918.

(67) Vreman, H. J., Schmitz, R. Y., and Skoog, F. (1974) Synthesis of 2-methylthio-*cis*- and *trans*-ribosylzeatin and their isolation from *Pisum tRNA*. *Phytochemistry* 13, 31–37.

(68) Lichtenthaler, F. W., Voss, P., and Heerd, A. (1974) Nucleosides, XX. Stannic Chloride catalyzed glycosidations of silylated purines with fully acylated sugars. *Tetrahedron Lett.* 15, 2141–2144.

(69) Ottria, R., Casati, S., Manzocchi, A., Baldoli, E., Mariotti, M., Maier, J. A. M., and Ciuffreda, P. (2010) Synthesis and evaluation of in vitro anticancer activity of some novel isopenenyladenosine derivatives. *Bioorg. Med. Chem.* 18, 4249–4254.

(70) Jordan, A., Pontis, E., Atta, M., Krook, M., Gibert, I., Barbe, J., and Reichard, P. (1994) A second class I ribonucleotide reductase in Enterobacteriaceae: characterization of the *Salmonella typhimurium* enzyme. *Proc. Natl. Acad. Sci. U. S. A.* 91, 12892–12896.

(71) Fox, B. G., Shanklin, J., Ai, J., Loehr, T. M., and Sanders-Loehr, J. (1994) Resonance Raman evidence for an Fe-O-Fe center in stearoyl-ACP desaturase. Primary sequence identity with other diiron-oxo proteins. *Biochemistry* 33, 12776–12786.

(72) Xiong, J., Phillips, R. S., Kurtz, D. M., Jr., Jin, S., Ai, J., and Sanders-Loehr, J. (2000) The O_2 binding pocket of myohemerythrin: role of a conserved leucine. *Biochemistry* 39, 8526–8536.

(73) Merckx, M., Kopp, D. A., Sazinsky, M. H., Blazyk, J. L., Müller, J., and Lippard, S. J. (2001) Dioxygen activation and methane hydroxylation by soluble methane monooxygenase: a tale of two irons and three proteins. *Angew. Chem., Int. Ed. Engl.* 40, 2782–2807.

(74) Kao, W. C., Wang, V. C., Huang, Y. C., Yu, S. S., Chang, T. C., and Chan, S. I. (2008) Isolation, purification and characterization of hemerythrin from *Methylococcus capsulatus* (Bath). *J. Inorg. Biochem.* 102, 1607–1614.

(75) Xiong, J., Kurtz, D. M., Jr., Ai, J., and Sanders-Loehr, J. (2000) A hemerythrin-like domain in a bacterial chemotaxis protein. *Biochemistry* 39, 5117–5125.

(76) Lei, Q. P., Cui, X., Kurtz, D. M., Amster, I. J., Chernushevich, I. V., and Standing, K. G. (1998) Electrospray mass spectrometry studies of non-heme iron-containing proteins. *Anal. Chem.* 70, 1838–1846.

(77) Broadwater, J. A., Ai, J., Loehr, T. M., Sanders-Loehr, J., and Fox, B. G. (1998) Peroxidiferic intermediate of stearoyl-acyl carrier protein delta 9 desaturase: oxidase reactivity during single turnover and implications for the mechanism of desaturation. *Biochemistry* 37, 14664–14671.

(78) Sjöberg, B. M., Karlsson, M., and Jornvall, H. (1987) Half-site reactivity of the tyrosyl radical of ribonucleotide reductase from *Escherichia coli*. *J. Biol. Chem.* 262, 9736–9743.

(79) Ge, J., Perlstein, D. L., Nguyen, H. H., Bar, G., Griffin, R. G., and Stubbe, J. (2001) Why multiple small subunits (Y2 and Y4) for yeast ribonucleotide reductase? Toward understanding the role of Y4. *Proc. Natl. Acad. Sci. U. S. A.* 98, 10067–10072.

(80) Sommerhalter, M., Voegtli, W. C., Perlstein, D. L., Ge, J., Stubbe, J., and Rosenzweig, A. C. (2004) Structures of the Yeast Ribonucleotide Reductase Rnr2 and Rnr4 Homodimers. *Biochemistry* 43, 7736–7742.

(81) Cherayil, J. D., and Lipsett, M. N. (1977) Zeatin ribonucleosides in the transfer ribonucleic acid of *Rhizobium leguminosarum*, *Agrobacterium tumefaciens*, *Corynebacterium fascians*, and *Erwinia amylovora*. *J. Bacteriol.* 131, 741–744.